Quantifying charge state heterogeneity for proteins with multiple ionizable residues

Martin J. Fossat, Ammon E. Posey, and Rohit V. Pappu*

Department of Biomedical Engineering and Center for Science & Engineering of Living Systems (CSELS), Washington University in St. Louis, St. Louis, MO 63130, USA

*Correspondence: pappu@wustl.edu

ABSTRACT

For proteins with multiple ionizable residues, the canonical assumption is that ionization states of residues are fixed by their intrinsic pK_a values. However, several studies have shown that protonation / deprotonation of acidic vs. basic sidechains is realizable even when the solution pH is kept fixed at values that are far away from the intrinsic pK_a values. Indeed, protein solutions are best described as ensembles of charge microstates, with each member of the ensemble being a distinct charge microstate defined by differences in charge states for ionizable residues. Accordingly, for a given set of solution conditions, the true partition function is sum over all charge microstates *and* all the Boltzmann weights of all conformations associated with each of the charge microstates. Here, we leverage the advantages afforded by potentiometric titrations to measure global net charge as a function of pH, independent of considerations of conformational preferences. The systems studied are fragments of proteins with repetitive patterns of Lys and Glu. We analyze the potentiometry data using the recently introduced formalism of the *q*-canonical ensemble. In this ensemble, charge microstates can be grouped into mesostates. Each mesostate is a collection of microstates of the same net charge. We analyze data for global charge vs. pH to extract mesostate populations as a function of pH. Our findings reveal that the heterogeneity of charge states makes significant contributions to measured charge profiles. This has significant implications for the types of species that are present in solution, even for a fixed pH. Measurements of net charge, decoupled from measurements of conformational equilibria, and analyzed to extract the pH-dependent populations of different mesostates, will be significant for accurate understanding of how charge state heterogeneity contributes to conformational, binding, and phase equilibria of proteins, especially those that are intrinsically disordered.

STATEMENT OF SIGNIFICANCE

Is the net charge of a protein fixed for a given set of solution conditions or is a heterogeneous distribution of charge states required to account for all thermodynamically relevant species? To answer this question, we carried out measurements of net charge as a function of pH using potentiometric titrations, which quantify the buffering capacity of a protein solution. The measured profiles of net charge vs. pH were analyzed for archetypal sequences using the recently introduced formalism of the *q*-canonical ensemble. We find that heterogeneous distributions of charge states contribute significantly to the charge profiles of proteins with multiple ionizable residues. We propose that charge state heterogeneities, realizable even at fixed pH, are likely to be important for protein function.

INTRODUCTION

Ionizable residues make key contributions to protein structure and function (1-6). They influence protein stability, solubility, and interactions mediated by the surfaces of the folded states of intrinsically foldable proteins (7-15), specifically in active sites of enzymes (16-18). Ionizable residues also feature prominently in intrinsically disordered proteins (IDPs) (19, 20). Indeed, several studies have documented the important contributions made by ionizable residues to conformational (21-26), binding (27-33), and phase equilibria of IDPs (34-42).

The charge states of ionizable residues are not fixed. Instead, they are regulated or altered through a variety of mechanisms that are collectively known as *charge regulation* (43-45). Active processes enable charge regulation through enzyme catalyzed reactions that lead to a variety of post-translational modifications (46) such as lysine acetylation (47), arginine citrullination (48), serine / threonine / tyrosine phosphorylation (49-51), and deamidation of asparagine / glutamine

(52). Each of these modifications alters the charge state of the residue in question. In addition to enzyme catalyzed charge regulation, the charge states of ionizable residues can also be altered by spontaneous processes such as site-specific binding / release of protons (2, 3, 7, 53-59), and the preferential accumulation or exclusion of solution ions around regions of high charge density (60-67). Accordingly, for a given set of solution conditions, the sequence of a protein is best described as an ensemble of charge states. Spontaneous alterations to the charges of ionizable residues become generators of the sequence- and solution condition-specific ensemble of charge states. Our focus in this work is on quantifying the effect of proton binding and release on the diversity of charge states that are thermodynamically accessible to proteins as a function of pH while keeping all other parameters of the solution fixed.

The charge states of ionizable residues are influenced by a combination of sequence contexts, solution conditions, and the linked effects of conformational equilibria (68, 69). As we will discuss below, the heterogeneity of charge states implies that a specific protein sequence is an ensemble of charge microstates, with each microstate being a distinct sequence defined by the charge states for ionizable residues. The ensemble of microstates can be reduced to a single microstate by assuming that the charge states are defined exclusively by the intrinsic pK_a values of amino acids. Accordingly, for "physiologically relevant solution conditions" (pH 7.4, 37˚C, and 100-300 mOsm of salts and solutes), one typically assumes that the bases Lys and Arg carry a charge of +1, the acids Asp and Glu carry a charge of -1, and His is neutral. Almost all experimental data are analyzed using this assumption. Likewise, molecular simulations are typically performed using fixed charge models. The validity of the fixed charge / single charge microstate assumption is seldom scrutinized, as this requires independent measurements of charge that are decoupled from measurements of conformational and / or binding equilibria.

We recently introduced the so-called *q*-canonical ensemble to account for charge state heterogeneity and assess the contributions of different charge states to conformational equilibria of peptides (70). The *q*-canonical ensemble refers to the ensemble of charge microstates *and* the conformations associated with each of the microstates (70). Therefore, the true partition function is a sum over all charge microstates *and* all conformations associated with each of the charge microstates. In the *q*-canonical ensemble, charge microstates can be grouped into *mesostates*, where each mesostate is a collection of microstates of the same charge. Accordingly, each mesostate is given a label q_k, where q is the net charge associated with each microstate within a mesostate, and k is the number of distinct, thermodynamically accessible microstates within the mesostate. An illustration of the *q*-canonical ensemble is shown in **Figure 1** for a simple peptide with two ionizable residues.

In this work, we leverage the *q*-canonical ensemble, specifically the grouping of charge microstates into mesostates (70), to quantify the pH dependence of mesostate populations. We achieve this by analyzing measurements of global charge, accessed via potentiometry, and the formalism afforded by the *q*-canonical ensemble. The result is a direct quantification of mesostate populations as a function of pH. Our findings reveal that the heterogeneity of charge states makes a major contribution to global charge profiles. The key takeaway is that measurements of conformational, binding, or phase equilibria, without independent measurements of charge and inferring the populations of different mesostates, will engender simplifying assumptions that are of questionable accuracy.

In the following sections, we summarize the challenges posed by acid-base equilibria of proteins with multiple ionizable residues. Such systems are also referred to as polyacids (54, 71-

74). We describe the *q*-canonical formalism and explain how this can be interfaced with potentiometric measurements (75-77). We then present results from our application of the *q*-canonical formalism to analyze potentiometry data for three model systems that are repeats of Lys and Glu. We conclude with a discussion of the broader implications of our findings, the general use of our approach, and the insights that will be forthcoming through joint use of the *q*-canonical ensemble, conformational sampling, and separate measurements of proton binding and conformational equilibria.

THEORY

The *q*-canonical ensemble: For a sequence with n ionizable residues, there are, in theory, 2^n distinct charge microstates to consider. However, for sequences that are mixtures of acids and bases, the number of thermodynamically relevant charge microstates can be significantly reduced by eliminating so-called forbidden states (70). This is because the intrinsic pK_a values are such that the protonation of acids and deprotonation of bases are unlikely to occur simultaneously. Any microstate that involves neutral versions of acidic and basic residues can, to first approximation, be ignored as forbidden microstates. Following the pruning of forbidden microstates, the number of thermodynamically relevant charge microstates that become states of interest for the calculation of partition functions is designated as Ω_{micro}. Even with pruning to eliminate forbidden microstates, Ω_{micro} will increase exponentially with the number of ionizable residues n. However, grouping microstates into mesostates, based on their net charge, leads to a considerable simplification as far as the ensemble of charge states is concerned.

A mesostate is made up of all charge microstates that have the same net charge. Each mesostate is assigned a label q_k where q denotes the net charge associated with each microstate within the mesostate and k denotes the total number of microstates within the mesostate. For example, the designation of $+1_3$ implies that there are three microstates in the mesostate, and all these microstates have a net charge of +1. The total number of mesostates, denoted as N_{meso}, scales linearly with the number of ionizable residues. The grouping of microstates into mesostates is useful for numerical analysis of potentiometric data. For emphasis, we take a detour through acid-base equilibria for simple systems vs. polyacids, showing how the large number of charge microstates must be accounted for when assessing pH-dependent titrations for polyacids.

Defining distinct types of pK_a values: For a monoacid such as a single glutamic acid, the pK_a is defined for the reaction $\mathrm{e} \rightleftharpoons \mathrm{E} + \mathrm{H}^+$. Here, e and E, respectively denote the protonated and deprotonated versions of Glu, and H^+ refers to the proton that is released upon deprotonation. The standard state ionization free energy for this simple reaction is defined as: $\Delta G^0 = -RT\ln\left(\frac{[\mathrm{E}][\mathrm{H}^+]}{[\mathrm{e}]}\right) = \ln(10)(\mathrm{pK_a})$. The picture becomes more complicated for polyacids because of the increase in the number of reactions that involve the loss of a proton (78). To illustrate this point, we shall consider the case of ac-$(Glu)_2$-nme, where ac and nme, respectively refer to N-acetyl and N′-methylamide. There are four separate reactions that involve the loss of a single proton. These are:

$$\begin{aligned} \text{ee} &\rightleftharpoons \text{eE} + \text{H}^+ \\ \text{ee} &\rightleftharpoons \text{Ee} + \text{H}^+ \\ \text{Ee} &\rightleftharpoons \text{EE} + \text{H}^+ \\ \text{eE} &\rightleftharpoons \text{EE} + \text{H}^+ \end{aligned} ; \tag{1}$$

Each of the reactions shown in Equation (1) can be assigned a pK_a. We refer to these as primary pK_a values, as they involve the loss of exactly one mole of protons from a single site for each mole of advancement of the reaction. For a system with Ω_{micro} microstates, there will be a set of $n2^{n-1}$ primary pK_a values. These cannot be measured, although they can be approximated (79-81). We can also use our notation for mesostates and rewrite the relevant reactions for the release of one mole of protons as follows:

$$\begin{aligned} 0_1 &\rightleftharpoons -1_2 + \text{H}^+ \\ -1_2 &\rightleftharpoons -2_1 + \text{H}^+ \end{aligned} ; \tag{2}$$

Here, $(0_1,-1_2)$ and $(-1_2,-2_1)$ constitute two pairs of adjacent mesostates. Adjacency refers to mesostates whose net charge differs by $\pm 1e$. Each reaction in Equation (2) can also be assigned a pK_a value. These mesostate pK_a values are different from the set of primary pK_a values. For N_{meso} mesostates, there will be $N_{meso} - 1$ mesostate pK_a values corresponding to transitions between pairs of adjacent mesostates. While the set of primary pK_a values cannot be measured, the set of mesostate pK_a values can be inferred from measurements of net charge as a function of pH, providing we are able to extract the pH-dependent populations of mesostates – a problem that we show can be solved through a blend of theory and experiment.

Accounting for charge state heterogeneity to quantify mesostate populations and the set of mesostate pK_a values: The use of fixed charge models in the analysis of experimental data or in molecular simulations relies on the assumption of unshifted pK_a values. There are several conceivable definitions of unshifted pK_a values. For the case of the ac-$(Glu)_2$-nme system, there are at least two distinct scenarios that could correspond to a seemingly reasonable definition of unshifted pK_a values. According to one assumption, the pK_a for a transition between two mesostates would be identical to the intrinsic pK_a. This would imply that $\Delta G_{q_k \to (q-1)_l} = \Delta G_{\text{e} \to \text{E}}$. However, this assumption is flawed because it ignores the number of reactions within a single mesostate, each involving a distinct microstate, that can contribute to the loss of a proton. The second model for unshifted pK_a values corresponds to the assumption that: $\Delta G_{\text{ee} \to \text{eE}} = \Delta G_{\text{e} \to \text{E}}$. This model assumes that the primary pK_a values can only be assigned to reactions involving individual microstates rather than collections of microstates. Here, the unshifted pK_a associated with transitions between mesostates can be derived through proper accounting of the diversity of charge microstates per mesostate. We illustrate these points using reactions for the ac-$(Glu)_2$-nme system. The mesostate -1_2 includes the microstates Ee and eE. Therefore, the concentration of mesostate -1_2, denoted as $[-1_2]$ is written as: $[-1_2] = [\text{Ee}] + [\text{eE}]$. Accordingly, the equilibrium constant for dissociation of a mole of protons from mesostate -1_2 is written as:

$$K = \frac{[-1_2]}{[\text{ee}]} = \frac{[\text{Ee}]+[\text{eE}]}{[\text{ee}]} = \frac{[\text{Ee}]}{[\text{ee}]} + \frac{[\text{eE}]}{[\text{ee}]} = \exp\left(-\frac{\Delta G_{\text{ee} \to \text{Ee}}}{RT}\right) + \exp\left(-\frac{\Delta G_{\text{ee} \to \text{eE}}}{RT}\right); \tag{3}$$

This allows us to identify the equilibrium constants that correspond to two primary pK_a values. Accordingly, the free energy of ionization of a single mesostate, for the specific example considered here, may be written as:

$$\Delta G^0_{0_1 \to -1_2} = -RT \ln\left[\exp\left(-\frac{\Delta G^0_{\text{ee}\to\text{Ee}}}{RT}\right) + \exp\left(-\frac{\Delta G^0_{\text{ee}\to\text{eE}}}{RT}\right)\right]; \quad (4)$$

If we assume that the primary pK_a values correspond to those of model compounds, we can use Equation (4) for polyacids by accounting for the number of microstates per each mesostate. The free energy of ionization that transforms mesostate q_k to $(q-1)_l$ of a polyacid, through the release of one mole of protons, may be written as:

$$\Delta G^0_{q_k \to (q-1)_l} = -RT \ln\left[\sum_{i=1}^{\Omega_{\text{micro},\,q_k}} \exp\left(-\frac{n_{q-1,i}\left(\Delta G^0_{\text{e}\to\text{E}}\right)_i}{RT}\right)\right] + RT \ln\left[\sum_{j=1}^{\Omega_{\text{micro},\,(q-1)_l}} \exp\left(-\frac{n_{q,j}\left(\Delta G^0_{\text{e}\to\text{E}}\right)_j}{RT}\right)\right]; \quad (5)$$

Here, $\Omega_{\text{micro},\,q_k}$ and $\Omega_{\text{micro},\,(q-1)_l}$ refer to the number of charge microstates within mesostates q_k and $(q-1)_l$, respectively; $\left(\Delta G^0_{\text{e}\to\text{E}}\right)_i$ and $\left(\Delta G^0_{\text{e}\to\text{E}}\right)_j$ are the context dependent free energies of ionization; $n_{q\text{-}1,i}$ and $n_{q,j}$ are the numbers of ionizable residues within microstates i and j that are in their basic forms. For example, $n_q = 1$ for microstates eE, eEe, kK, KKk, etc. Likewise, $n_q = 2$ for microstates eEE, kkK, etc. Here, k is the deprotonated version of lysine (K). For the transformation of mesostate 0_1 to mesostate -1_2, $n_{q\text{-}1,i} = 1$ for each of the microstates Ee and eE, whereas $n_{q,j} = 0$ for the microstate ee.

Equation (5) reduces to Equation (4) if we set $\Delta G^0_{\text{ee}\to\text{Ee}} = \left(\Delta G^0_{\text{e}\to\text{E}}\right)_i$ and $\Delta G^0_{\text{ee}\to\text{eE}} = \left(\Delta G^0_{\text{e}\to\text{E}}\right)_j$. If all microstates within a mesostate are equiprobable, implying that the ionization free energy is independent of sequence context, then Equation (5) reduces to:

$$\Delta G^0_{q_k \to (q-1)_l} = -RT \ln\left[\Omega_{\text{micro},q_k} \exp\left(-\frac{n_{q-1}\,\Delta G^0_{\text{e}\to\text{E}}}{RT}\right)\right] + RT \ln\left[\Omega_{\text{micro},(q-1)_l} \exp\left(-\frac{n_q\,\Delta G^0_{\text{e}\to\text{E}}}{RT}\right)\right]; \quad (6)$$

Upon further rearrangement, Equation (6) becomes:

$$\begin{aligned}\Delta G^0_{q_k \to (q-1)_l} &= \Delta G^0_{\text{e}\to\text{E}} - RT \ln\Omega_{\text{micro},q_k} + RT \ln\Omega_{\text{micro},(q-1)_l} \\ &= \Delta G^0_{\text{e}\to\text{E}} - TS_{\text{micro},q_k} + TS_{\text{micro},(q-1)_l}\end{aligned}; \quad (7)$$

Equation (7) highlights the importance of "sequence entropy" i.e., microstate entropy that features as two terms: $S_{\text{micro},q_k} = R\ln\Omega_{\text{micro},q_k}$ and $S_{\text{micro},(q-1)_l} = R\ln\Omega_{\text{micro},(q-1)_l}$. These are the microstate entropies of mesostates q_k and $(q-1)_l$, respectively. The implication is that even for the simple scenario of context-independent pK_a values, the free energy difference between a pair of adjacent mesostates, which is a measure of the pK_a associated with the transition between a pair of adjacent mesostates, must account for the contributions of different microstate entropies for each mesostate. In general, the microstate weights are likely to be non-identical. In this scenario, the pH-

independent standard state free energy change associated with transformation from mesostate q_k to $(q-1)_l$ is written as:

$$\Delta G^0_{q_k \to (q-1)_l} = -RT \ln\left[\sum_{i=1}^{\Omega_{\text{micro},(q-1)_l}} \exp\left(-\frac{\Delta G_i^0}{RT}\right)\right] + RT \ln\left[\sum_{j=1}^{\Omega_{\text{micro},q_k}} \exp\left(-\frac{\Delta G_j^0}{RT}\right)\right]; \quad (8)$$

Here, ΔG_i^0 is the standard state free energy of microstate *i*. In the following sections we show how potentiometry, which measures the buffering capacity of a solute as a function of pH, can be used in conjunction with Equation (8), to derive mesostate populations as a function of pH.

Extracting mesostate populations from potentiometry measurements: We use potentiometry to estimate the net charge of a protein as a function of pH. This is achieved by titrating the solution pH using a strong acid or a strong base. The buffering capacity of a protein solution, referenced to the buffering capacity of the protein-free solution, is used to estimate the profile of net charge vs. pH. Given the ensemble-averaged net charge vs. pH as an input, we can fit the measured profile to extract the pH-dependent population of mesostates. This information allows us to extract the contributions made by distinct mesostates to the pH-dependent net charge profile. The measured net charge q_{net} as a function of pH may be written as:

$$q_{\text{net}}(\text{pH}) = \sum_{i=1}^{N_{\text{meso}}} p_i(\text{pH}) q_i; \quad (9)$$

Here, q_i is the charge associated with mesostate *i* and p_i(pH) is the probability of populating mesostate *i* for a given pH. Given knowledge of q_{net}(pH), the charge associated with each mesostate, and intrinsic pK_a values derived from model compounds, we can estimate the pH-dependent mesostate probabilities by fitting the measured profiles to Equation (9). The fitting procedure is based on a Metropolis Monte Carlo method (82) that minimizes the deviation between the measured and estimated charge profile by minimizing a cost function defined as:

$$E_{\text{fit}} = \int \left| q_{\text{est}}(\text{pH}) - q_{\text{net}}(\text{pH}) \right| d\text{pH}; \quad (10)$$

Here, q_{est} and q_{net} are the estimated and measured net charge values for a given pH. The fitting procedure, summarized in **Figure 2**, is seeded by assigning mesostate probabilities using Equation (7). The intrinsic pK_a values we use are 10.7 for Lys and 4.34 for Glu (83). The parameter $\Delta_{\max}$ (see **Figure 2**) is set so that the maximal change in relative free energies of states i and j that are being perturbed will be no more than 0.01 kcal / mol. The Metropolis criterion for accepting or rejecting a proposed change in mesostate probabilities is of the form: $\min\left\{1, \exp\left(-\frac{\Delta E_{\text{fit}}}{T_{\text{fit}}}\right)\right\}$.

Here, ΔE_{fit} quantifies how the cost function E_{fit} has changed with the newly proposed mesostate probabilities. The parameter T_{fit} is a scalar parameter, which is a fictitious, albeit unitless, temperature that is chosen to enable efficient convergence of the Monte Carlo based fitting procedure. The optimal temperature will be system-specific, and is chosen by inspecting the acceptance ratio and making sure it is not close to one or below a numerical tolerance. Data from potentiometry measurements (see below) converted into profiles of net charge vs. pH are used to quantify how the mesostate probabilities evolve as a function of pH. Additional details regarding the Monte Carlo fitting procedure are available in the Supporting Material.

MATERIALS AND METHODS

Reagents and peptides: Potassium chloride (KCl), hydrochloric acid (HCl), potassium hydroxide (KOH), and potassium hydrogen phthalate (KHP) were purchased from Sigma. Peptides were purchased from GenScript at >95% purity as HCl salts with acetylated N-termini and amidated C-termini. Salt content was determined by mass spectrometry. Peptides were stored in lyophilized form at –20℃ in sealed containers in the presence of desiccant until they were used for experiments. We performed measurements for three repetitive peptides, excised from proteins with single alpha helical domains. The amino acid sequences of the three peptides were as follows: Ac-G-$(E_4K_4)_n$-GW-NH_2, where n = 1, 2, or 3. The peptides were capped at the N- and C-termini using N-acetyl (ace) and an amide, respectively. This avoids confounding effects from charged termini. Trp was used to enable precise measurements of concentration.

Sample preparation: A sealed flask of ultrapure water was depleted of CO_2 using a custom-built Schlenk line to apply alternating cycles of nitrogen gas and vacuum. The resulting CO_2 depleted water and all solutions and samples prepared from this water were kept in sealed flasks or vials and stored in a glove bag (AtmosBag, Millipore-Sigma Z530204) filled with nitrogen gas. All transfers of these liquids between flasks or vials were carried out within the nitrogen-filled glove bag or using gas-tight Hamilton syringes to access sealed vials without exposing the contents to air. A stock solution of background solvent was prepared by dissolving KCl in CO_2-depleted ultrapure water to which HCl had been added. The final solution contained 10 mM KCl and 5 mM HCl. This solution was further depleted of CO_2 using the Schlenk line, after which it was sealed and stored in a nitrogen-filled glove bag until further use.

A 50 mM KOH solution was used as the titrant for all potentiometry experiments. A 200 mM KOH stock solution was prepared in the glove bag using CO_2-depleted ultrapure water. This stock was further diluted to 50 mM KOH with CO_2-depleted ultrapure water and sealed in a glass vial with a Teflon-coated rubber septum while in the nitrogen-filled glove bag. Peptides were dissolved in the CO_2-depleted background solution at a concentration of ~200 μM. Immediately prior to each potentiometry experiment, the peptide concentration was measured by UV/visible spectroscopy using Trp absorbance at 280 nm and an extinction coefficient of 5500 M^{-1} cm^{-1}. A KHP solution at a concentration of 1 mM was prepared by massing a quantity of KHP powder into a glass vial using a precision mass balance, transferring the vial to the nitrogen-filled glove bag, and then adding CO_2-depleted ultrapure water directly to the vial to dissolve the material. The sample was stored in a sealed vial in the nitrogen-filled glove bag until further use.

Potentiometry: All measurements were carried out in a custom sample vial consisting of a glass screw-cap vial sealed with Teflon-coated rubber septum with a 5 mm hole (created with a biopsy punch) that accommodated the pH probe while still forming a seal. Titrant was delivered to the sealed vial through the rubber septum using a precision gas-tight μL syringe fitted with a repeating dispenser (Hamilton). Potentiometric measurements were carried out on an Orion Star A215 potentiometer (Thermo Scientific) using a pHT-micro combination probe with a platinum / Silamid double junction (YSI). A 2 mL sample was titrated with 50 mM KOH in 2 μL increments in all cases.

The concentration of the KOH solution was verified by titrating a known concentration of potassium hydrogen phthalate (KHP) having a well-documented pKa of 5.4, as follows: a 2 mL volume of KHP solution was titrated with ~50 mM KOH solution in 2 μL increments, and the pH of the solution was measured after each addition. A titration of 2 mL of background solution was

carried out in the same manner. The resulting potentiometry curves (KHP and background) were analyzed by Gran analysis (84, 85) as well as by first and second derivative analyses to determine the precise KOH concentration (86, 87).

For each peptide, a 2 mL volume of peptide solution was titrated with ~50 mM KOH solution in 2 μL increments, and the pH of the solution was measured after each addition. A titration of 2 mL of background solution was carried out in the same manner. For each peptide titration, the KOH solution used as titrant was prepared fresh and calibrated with a KHP titration as described above.

Calculation of peptide net charge: Since KOH is a strong base, we can assume that for each mole of OH added, one mole of protons is consumed, resulting in water as the product. Since the concentration of the KOH solution is known, it is straightforward to calculate the number of moles of KOH from the volume of KOH added. The difference in KOH volume added between the titration curves for peptide and background represents a quantity that is proportional to the moles of protons introduced by the peptide. Since the peptide concentration is known, we can readily calculate the number of protons per peptide. The number of protons released over the course of the titration is equivalent to the change in net charge of the peptide. Therefore, the net charge of the peptide can be determined as a function of pH if the net charge is known at the starting point of the titration. Since the peptide titration is started at a low pH (~2.0) that is below the pK_a of all ionizable groups present, we can assume that all ionizable groups are protonated, and the net charge on the peptide should be equal to the number of cationic residues, (Lys in the case of $(E_4K_4)_n$ peptides).

Following the approach pioneered by Nozaki and Tanford (88), the data were transposed to facilitate comparison of the volume of KOH added in the background titration vs. the peptide titration at each pH value (2, 89). A linear interpolation between each data point within a given titration curve was carried out so that the background curve could be subtracted from the peptide curve at any pH value. The resulting quantities represent the difference in KOH volume added in the background titration vs. the peptide titration at a given pH value. Multiplying these values by the known concentration of KOH gives the difference in number of moles of KOH between the two curves, and this is equivalent to the number of protons introduced by the peptide. Dividing this value by the number of moles of peptide (calculated as peptide concentration multiplied by sample volume) quantifies the moles of protons per moles of peptide, which is equivalent to relative change in net charge.

As explained above, for $(E_4K_4)_n$ peptides, the number of Lys residues provides the offset value needed to shift the calculated moles of protons per peptide to the appropriate register for reporting net charge of the peptide. In practice, there are a few sources of uncertainty that may require adjustments to both the scaling and the offset of the net charge curve. These include potential sources of uncertainty in measurements of concentration, and the presence of trace amounts of residual acid in the peptide sample. To account for these errors, we scale the protein net charge curve such that the inflection point around neutral pH has a charge of 0. This is the most parsimonious rescaling, since any other rescaling would lead to mesostates with non-zero charge being dominant population around pH 7.0, implying that the 0_1 mesostate would never be dominant in the ensemble. The rescaling factor used for each construct is 0.92, 0.76 and 0.79 for $(E_4K_4)_1$, $(E_4K_4)_2$, and $(E_4K_4)_3$, respectively.

RESULTS

Sequences with a consensus repeat consisting of $(E_4X_4)_n$ or $(E_3X_3)_n$ where X is either an Arg or Lys have been shown to form alpha helical conformations (90-93). These single alpha helix forming sequences are typically excised from larger proteins (92). Helicity is known to increase with the repeat length (90). The single alpha helices are thought to be useful in force transduction in myosin (91) and have been deployed as spectroscopic rulers for Förster resonance energy transfer measurements, *in vitro* and in cells (94). The overall helicity has been ascribed to a network of intra-helical salt bridges between residues i and i+4 (90, 93).

Here, we ask if a single mesostate *viz*., 0_1 dominates over the entire accessible pH range. This question is motivated by observations showing a remarkable stability of the alpha helical conformations across a wide range of pH values (93, 95). We reasoned that it is unlikely for networks of salt bridges to be operative under conditions where Glu is protonated, or Lys is deprotonated. A definitive assessment of the curious pH insensitivity requires knowledge of how the net charge varies with pH, and we measure this directly. We can then use these data, in conjunction with the *q*-canonical ensemble to infer the populations of each of the relevant mesostates as a function of pH. The measurements reveal a series of insights that are summarized next.

Fitting of potentiometric data: Figure 3A, B, and C show the quality of the fits obtained for each of the three peptides. In each panel, the gray circles denote the raw experimental data that are not used in the fitting procedure. The orange points are the raw data used for the fitting procedure. The fitting procedure was applied to the smoothed version of the data to have a uniform resolution across the pH range to ensure that evaluation of the cost function is uniformly distributed. The raw data and comparisons to the smoothed data are shown in **Figure S1**. Fits to the data are shown using two models, depicted using blue vs. red curves. The red curves are charge profiles calculated using Equation (7), which assumes model compound pK_a values for all the ionizable residues, although the microstate entropies per mesostate are different. In this model, the only parameters that distinguish different mesostates are net charge and the microstate entropy per mesostate. These fits, which do not describe the data well, clearly indicate that there are shifted pK_a values in each of the three sequences. The blue curves show the quality of fit obtained through the Monte Carlo fitting procedure. The quality of the fits is shown in terms of residuals included at the bottom of each panel. The mesostate probabilities change with respect to the unshifted model, and these changes are reflected in the improved fits to the net charge vs. pH profiles. We further assessed the quality of the fits by calculating the pH-dependent derivatives of the net charge profiles, for the experimental data and for the numerical fits. These comparisons are shown in **Figure S2**. **Figure 3D** shows a comparison of the normalized net charge vs. pH for the three peptides. If the unshifted model were to be valid, then the three curves should collapse on one another. Clearly, this is not the case, and it points to a sequence- and hence context-dependent contribution for the increasing diversity of mesostates with peptide length.

Given the widespread use of fixed charge models, we also compared charge profiles calculated using this model to the measured profiles from potentiometry. Here, we assume that Lys is always protonated below its intrinsic pK_a and Glu is always deprotonated above its intrinsic pK_a. The results are shown in the three panels of **Figure 4**. Again, each panel includes the gray circles, orange points, and blue curves that are identical to those in **Figure 3**. The black curves in each of the three panels show the charge profiles that we compute using the fixed charge model. Clearly, the fixed charge model does not accurately recapitulate how the measured charge varies with pH, at least for the $(E_4K_4)_n$ series of peptides.

Interpretations from the measured charge profiles: The profile for (E_4K_4) shows a plateau in the pH range between 7 and 9 (**Figure 3a**). This observation is confirmed by calculations of the derivative as a function of pH, which show that the derivative is essentially zero in the pH range between 7 and 9 (**Figure S2a**). The implication is that none of the acids or bases are titrating their charge states in this pH range. Therefore, a single mesostate must be dominant in this pH range for the E_4K_4 peptide. It is noteworthy, however, that the plateau region of the blue curve in **Figure 3a** is larger than that of the red curve. The latter corresponds to the model that uses unshifted, model compound pK_a values while accounting for differences in microstate entropies of the different mesostates. Thus, the data indicate a downshift vs. an upshift in the pK_a values for the acids and the bases, respectively. In contrast to the (E_4K_4) peptide, the two longer peptides $(E_4K_4)_2$ and $(E_4K_4)_3$ do not have a pH range where the charge profile plateaus (**Figures 3b** and **3c**), and this is confirmed by the absence of a pH region where the derivative is zero (**Figures S2b** and **S2c**). This suggests that at every pH, there is at least more than one mesostate (and hence microstate) that contributes to the measured charge profiles, especially for $(E_4K_4)_2$.

Insights from pH-dependent mesostate populations: Fitting of the data for net charge vs. pH using the *q*-canonical ensemble formalism, specifically Equation (7), yields the pH-dependence of mesostate populations. The results are shown in **Figures 5-7** for E_4K_4, $(E_4K_4)_2$, and $(E_4K_4)_3$, respectively. The dashed vertical lines in **Figure 5** help quantify mesostate pK_a values. For E_4K_4, the $+1_4$ and 0_1 mesostates have equal likelihoods of being populated at a pH of 4.99. This implies that the pK_a associated with the transition between $+1_4$ and 0_1 mesostates is 4.99. Using a similar approach, we find that the pK_a value associated with the transition between 0_1 and -1_8 mesostates is 11.32. Therefore, the 0_1 mesostate is dominant within the pH range between 4.99 and 11.32, with the gap between the two mesostate pK_a values being 6.33 pH units. However, the dominance of the 0_1 mesostate weakens with increasing numbers of E_4K_4 repeats. Instead, the prominence of the mesostates with net charges of ±1 increases with the number of E_4K_4 repeats.

For $(E_4K_4)_2$ the pK_a values for the transitions $+1_8 \leftrightarrow 0_1$ and $0_1 \leftrightarrow -1_8$ are 5.34 and 8.80, respectively (**Figure 6**) implying a gap of 3.46 pH units. This gap between the two pK_a values corresponding to transitions between 0_1 and its adjacent mesostates further narrows for $(E_4K_4)_3$ (**Figure 7**). Here, the pK_a values for the transitions $+1_{12} \leftrightarrow 0_1$ and $0_1 \leftrightarrow -1_{12}$ are 6.14 and 9.01, respectively (gap of 2.87 pH units). The mesostate pK_a for transitions between the mesostate with net charge +1 and the 0_1 mesostate shifts up with increasing numbers of repeats. In contrast, the pK_a for transitions between the mesostate with net charge -1 and 0_1 shows non-monotonic variation with the number of repeats. This derives from the steeper variation of net charge with pH as the intrinsic pK_a of Lys is approached. In contrast, the mesostate with charge +1 is accessible in a pH range where the net charge shows a weaker pH dependence.

The gap between pK_a values for transitions between the 0_1 and adjacent mesostates that have a net charge of ±1 narrows from 6.33 to 3.46 and 2.87 pH units as the number of E_4K_4repeats increases from 1 to 2 to 3. It is likely that this gap further narrows as the numbers of repeats increase. One of the main takeaways is that for $(E_4K_4)_3$, the mesostate $+1_{12}$ contributes significantly, in addition to the 0_1, mesostate at pH 7.0 (see pink line in **Figure 7**). This contribution weakens in favor of the -1_{12} mesostate as the pH increases above 7.4. Therefore, even at pH 7.0, there are at least 13 distinct microstates whose contributions to the conformational ensemble must be considered.

The importance of charge state heterogeneity increases as the pH increases or decreases from the value of 7.0. The pH dependent populations of mesostates can be used to quantify the

numbers of mesostates that contribute to 95% vs. 99% of the overall population as a function of pH. The results are summarized in **Figure 8**. **Figure 8A** shows that a single mesostate, 0_1, and hence a single microstate, contributes to 99% of the population for the E_4K_4 peptide across a wide pH range. For the $(E_4K_4)_2$, 2-3 mesostates are required to account for the 90-99% of the preferred mesostates between the pH range of 7-9 (**Figure 8B**). We obtain similar results for the $(E_4K_4)_3$ system (**Figure 8C**). It follows that an explanation of the apparent insensitivity of helicity to changes in pH might derive from the helicity associated with microstates that have a net charge. In this scenario, it cannot just be the network of salt bridges that contribute to stabilizing helical conformations. Instead, the interplay among differences in free energies of solvation of charged and neutral forms of Glu and Lys (96) as well as the higher intrinsic helical propensity of neutral Glu vs. charged Glu (97-100) are likely contributors to the intriguing robustness of measured helicities to large-scale changes in pH. Accounting for the totality of these interactions requires a combination of charge measurements, presented here, and measurements of conformational equilibria, that are jointly used in a suitable molecular simulation framework for describing the total *q*-canonical ensemble.

DISCUSSION

Here, we have highlighted the importance of charge state heterogeneity that mandates the use of a *q*-canonical ensemble to describe how net charge varies with pH across a wide range of pH values. Our results are likely to be of particular interest for uncovering the dual impacts of charge state and conformational heterogeneity for IDPs, as these systems tend to be rich in ionizable residues, with a large fraction featuring more than 30% of ionizable residues (19). This number increases when we include the contributions of neutral residues that become ionizable following post-translational modifications such as Ser / Thr phosphorylation. Well-known IDPs include the prothymosin α system that has been studied extensively by the Schuler group (27, 101-106) as well as acid-rich disordered proteins that function as transactivation domains of transcription factors (107). These systems are among the closest mimics of homo polyacids, which are seldom fully deprotonated in solution (53, 54). Interestingly, single molecule electrometry measurements performed by Ruggeri et al., (105) suggest that only 28.5 ± 1.2 out of the 46 D/E residues in prothymosin α are, on average, deprotonated at pH 8.8. Given the growing interest in the conformational, binding (108), and phase equilibria of polyampholytic, polyzwitterionic (109, 110), and polyelectrolytic IDPs (111), it becomes imperative that measurements of net charge and extraction of mesostate populations using the *q*-canonical ensemble formalism be performed for a cross section of IDPs.

Features of the *q*-canonical ensemble: This ensemble has multicanonical (112) and grand canonical (113) characters. The multicanonical character (112) comes from the fact that each q_k mesostate combines the contributions of canonical ensembles of k distinct microstates. The *q*-canonical ensemble also has a grand canonical character (113) because it combines the contributions of all possible mesostates, each distinguished by net charge. Accordingly, for a given pH, any experimentally measured readout will be a weighted average over each thermodynamically relevant microstate *and* the conformational ensembles for each of these microstates.

The structure of the *q*-canonical ensemble allows us to decouple measurements of charge from measurements of conformation. Using this decoupling, specifically the mesostate description of the net charge extracted from the *q*-canonical ensemble, shown in Equation (7), we analyze potentiometry-based charge profiles as a function of pH to quantify the number and types of

mesostates that are thermodynamically relevant for a given set of solution conditions. We find that microstate entropy per mesostate makes significant contributions to the distribution of thermodynamically accessible mesostates. Importantly, the contributions of microstate entropy grow with the number of ionizable residues. Whether or not this heterogeneity can be overcome by dominant conformational preferences of specific microstates can only be decided by decoupling the measurements of charge from other readouts such as measurements of conformation and / or binding.

It is worth emphasizing the intrinsic differences between a site-specific representation of ionizable groups, and a description in terms of mesostates afforded by the *q*-canonical ensemble. If one were to measure pK_a values using site-specific titrations, aided by appropriate spectroscopic approaches such as nuclear magnetic resonance (NMR) (8, 81, 114) or infrared (IR) spectroscopy (99), the inferred variations in site-specific pK_a values would be much lower than the variations that we can unmask by the mesostate representation, which require measurements of global charge profiles.

Potentiometry: The simplicity of potentiometric titrations is key to its robustness (115). The buffering capacity can be measured to obtain net charge profiles as a function of pH by fixing solution conditions such as salt concentration, salt type, and the solution temperature. Therefore, with suitable automation, potentiometry can provide direct access to charge profiles as a function of pH for a range of systems and solution conditions. These data, when analyzed using the *q*-canonical formalism, will be essential for understanding the extent of sequence- and composition-specific effects of charge regulation via proton binding and release.

Being one of the earliest methods to characterize acid-base equilibria in chemical species, several methods for the interpretation of potentiometric curves, especially for monoacids, have been developed (115). However, the interpretation of potentiometric data has remained an unsolved problem for polyacids (54). We propose that our *q*-canonical ensemble-based approach provides an alternative route and complete description of the measured charge profiles.

Historically, potentiometry measurements have been used to assess the presence of anomalous or shifted pK_a values (2). This is typically achieved by using model compound pK_a values, ignoring the microstate entropy, and querying whether the measured net charge profiles match or deviate from the calculated profiles. The qualitative assessments from analysis of potentiometry are typically used to set up detailed site-specific measurements of local pK_a values using NMR spectroscopy or other types of spectroscopies that rely on isotopic labeling at specific sites.

The net charge profiles extracted using potentiometry have also been analyzed by prescribing model conformations and the calculation of conformation-specific electrostatic potentials. The goal in these endeavors is to assess the extent to which local sequence contexts can be implicated as modifiers of local pK_a values that cause deviations of measured charge profiles from expectations based on model compounds. While these efforts highlight the importance of charge regulation, they ignore the contributions of microstate entropy. Here, we leverage the mesostate groupings afforded by the *q*-canonical ensemble description and show how this can be deployed to extract insights regarding the pH-dependence of mesostate populations.

Potentiometry vs. other methods to measure charge: Methods to measure charge are of considerable interest, especially for the study of IDPs. Several methods such as capillary electrophoresis (57, 116) and single molecule electrometry (105) have been introduced and

deployed for measuring the net charges of IDPs and other flexible polymers. A limitation of these methods is the reliance on measurements of molecular mobility in the presence of a potential drop or a spatially patterned electric field. Analysis of data from such mobility-based measurements requires the *a priori* assumption of a preferred conformational state. Further complications arise because electrophoretic mobility measurements require the use of ultra-low salt concentrations to avoid confounding effects on mobilities that arise from the adsorption or release of solution ions. Accordingly, we propose that potentiometry might be the preferred approach for independent measurements of charge.

Summary and prognosis: We have introduced a theoretical formalism, leveraging the recently introduced q-canonical ensemble, to analyze potentiometric titrations. We showcase the approach using measurements and analyses for three related systems. The formalism is applicable for analyzing multisite binding isotherms (117-119) for arbitrary ligands, not just protons. Our results highlight the importance of charge state heterogeneity and the fact that the importance of heterogeneity grows with the number of ionizable residues. Potentiometric measurements, combined with separate measurements of the pH dependence of conformational ensembles, can be analyzed using the q-canonical ensemble to extract mesostate populations as well as microstate populations. The latter is being pursued for a series of systems, using sampling methods developed for the q-canonical ensemble (70). The results, which will be published elsewhere, will likely move us in the direction of quantifying the extent to which charge state and conformational heterogeneity either enhance or antagonize one another. These studies are likely to be of crucial importance for understanding and modeling the conformational, binding, and phase equilibria of IDPs. Such studies take on additional significance given various observations of pH-responsive equilibria for IDPs (42), recent measurements highlighting the significant extent of charge regulation in polyelectrolytic IDPs, and the presence of compartments of highly variable pH environments within cells.

AUTHOR CONTRIBUTIONS

Conceptualization: M.J.F., and R.V.P. Development of the formal theory and analysis: M.J.F. Potentiometry setup, troubleshooting, and measurements: A.E.P. Numerical analysis of potentiometry data: M.J.F., and R.V.P. Writing of the manuscript: M.J.F., and R.V.P. Editing: M.J.F., A.E.P., and R.V.P. Funding: R.V.P.

ACKNOWLEDGMENTS

We thank Furqan Dar, Mina Farag, Andrew Lin, Kiersten Ruff, Min Kyung Shinn, and Xiangze Zeng for careful reading of the manuscript. This work was supported by grant FA9550-20-1-0241 from the Air Force Office of Scientific Research, grants R01NS089932 and 5R01NS056114 from the US National Institutes of Health, and the St. Jude Children's Research Collaborative on Membraneless Organelles.

LIST OF FIGURES

Figure 1: Schematic showing charge microstates and the grouping into mesostates for ac-(Glu)$_2$-nme. Here ace and nme refer to N-acetyl and N′-methylamide, respectively. Protonated and deprotonated Glu residues are depicted as e and E, respectively. The charge microstates ee, eE, Ee, and EE can be grouped into mesostates, and the designation of mesostates, shown in q_k format is shown in purple.

Figure 2: Flowchart summarizing the workflow for fitting data from potentiometric titrations to Equation (9).

Figure 3: Raw data and results obtained from fitting the model based on unshifted pK_a values vs. the full model – Equation (9) – to the profile of net charge vs. pH obtained from potentiometric titrations. Panel (D) shows a comparison of the fitted profiles for the three peptides. To enable these comparisons, the ordinate is rescaled to be normalized by the magnitude of the maximal charge realizable for each system.

Figure 4: Comparison of the raw data, fits obtained using the full model, and a model that uses fixed charges. The results are shown for each of the three peptides. In each panel, the black curve corresponds to the fixed charge model. This model does a poor job of recapitulating the titration curve.

Figure 5: Mesostate probabilities, plotted against pH, for the E_4K_4 peptide. The dashed lines in each panel mark the pH values at which mesostates adjacent to the 0_1 mesostate have equal likelihoods of being populated. The pink line in each panel corresponds to a pH of 7.0.

Figure 6: Mesostate probabilities, plotted against pH, for the $(E_4K_4)_2$ peptide. The dashed lines in each panel mark the pH values at which mesostates adjacent to the 0_1 mesostate have equal likelihoods of being populated. The pink line in each panel corresponds to a pH of 7.0.

Figure 7: Mesostate probabilities, plotted against pH, for the $(E_4K_4)_3$ peptide. The dashed lines in each panel mark the pH values at which mesostates adjacent to the 0_1 mesostate have equal likelihoods of being populated. The pink line in each panel corresponds to a pH of 7.0.

Figure 8: Minimum number of mesostates that are required to account for 95% and 99% of the population, as a function of pH, for each of the three peptides.

REFERENCES

1. Pace, C. N., G. R. Grimsley, and J. M. Scholtz. 2009. Protein Ionizable Groups: pK Values and Their Contribution to Protein Stability and Solubility. Journal of Biological Chemistry 284:13285-13289.

2. Whitten, S. T., and E. B. Garcia-Moreno. 2000. pH dependence of stability of staphylococcal nuclease: evidence of substantial electrostatic interactions in the denatured state. Biochemistry 39:14292-14304.

3. Whitten, S. T., J. O. Wooll, R. Razeghifard, E. B. Garcia-Moreno, and V. J. Hilser. 2001. The origin of pH-dependent changes in m-values for the denaturant-induced unfolding of proteins. Journal of molecular biology 309:1165-1175.

4. Castle, P. E., D. A. Karp, L. Zeitlin, E. B. Garcia-Moreno, T. R. Moench, K. J. Whaley, and R. A. Cone. 2002. Human monoclonal antibody stability and activity at vaginal pH. Journal of reproductive immunology 56:61-76.

5. Mehler, E. L., M. Fuxreiter, I. Simon, and E. B. Garcia-Moreno. 2002. The role of hydrophobic microenvironments in modulating pKa shifts in proteins. Proteins: Structure, Function, Bioinformatics 48:283-292.

6. Schlessman, J. L., C. Abe, A. Gittis, D. A. Karp, M. A. Dolan, and E. B. Garcia-Moreno. 2008. Crystallographic study of hydration of an internal cavity in engineered proteins with buried polar or ionizable groups. Biophys J 94:3208-3216.

7. Whitten, S. T., E. B. Garcia-Moreno, and V. J. Hilser. 2005. Local conformational fluctuations can modulate the coupling between proton binding and global structural transitions in proteins. Proc Natl Acad Sci U S A 102:4282-4287.

8. Castaneda, C. A., C. A. Fitch, A. Majumdar, V. Khangulov, J. L. Schlessman, and B. E. Garcia-Moreno. 2009. Molecular determinants of the pKa values of Asp and Glu residues in staphylococcal nuclease. Proteins 77:570-588.

9. Harms, M. J., C. A. Castaneda, J. L. Schlessman, G. R. Sue, D. G. Isom, B. R. Cannon, and E. B. Garcia-Moreno. 2009. The pK(a) values of acidic and basic residues buried at the same internal location in a protein are governed by different factors. Journal of molecular biology 389:34-47.

10. Isom, D. G., C. A. Castaneda, B. R. Cannon, P. D. Velu, and E. B. Garcia-Moreno. 2010. Charges in the hydrophobic interior of proteins. Proceedings of the National Academy of Sciences of the United States of America USA 107:16096-16100.

11. Kitahara, R., K. Hata, A. Maeno, K. Akasaka, M. S. Chimenti, E. B. Garcia-Moreno, M. A. Schroer, C. Jeworrek, M. Tolan, R. Winter, J. Roche, C. Roumestand, K. Montet de Guillen, and C. A. Royer. 2011. Structural plasticity of staphylococcal nuclease probed by perturbation with pressure and pH. Proteins 79:1293-1305.

12. Peck, M. T., G. Ortega, J. N. De Luca-Johnson, J. L. Schlessman, A. C. Robinson, and E. B. Garcia-Moreno. 2017. Local Backbone Flexibility as a Determinant of the Apparent pKa Values of Buried Ionizable Groups in Proteins. Biochemistry 56:5338-5346.

13. Petrosian, S. A., and G. I. Makhatadze. 2000. Contribution of proton linkage to the thermodynamic stability of the major cold-shock protein of Escherichia coli CspA. Protein science : a publication of the Protein Society 9:387-394.

14. Permyakov, S. E., G. I. Makhatadze, R. Owenius, V. N. Uversky, C. L. Brooks, E. A. Permyakov, and L. J. Berliner. 2005. How to improve nature: study of the electrostatic properties of the surface of alpha-lactalbumin. Protein Engineering Design and Selection 18:425-433.

15. Chan, C. H., C. C. Wilbanks, G. I. Makhatadze, and K. B. Wong. 2012. Electrostatic contribution of surface charge residues to the stability of a thermophilic protein: benchmarking experimental and predicted pKa values. PloS one 7:e30296.

16. Hofer, F., J. Kraml, U. Kahler, A. S. Kamenik, and K. R. Liedl. 2020. Catalytic Site pKa Values of Aspartic, Cysteine, and Serine Proteases: Constant pH MD Simulations. Journal of chemical information and modeling 60:3030-3042.

17. Bartlett, G. J., C. T. Porter, N. Borkakoti, and J. M. Thornton. 2002. Analysis of Catalytic Residues in Enzyme Active Sites. Journal of molecular biology 324:105-121.

18. Harris, T. K., and G. J. Turner. 2002. Structural Basis of Perturbed pKa Values of Catalytic Groups in Enzyme Active Sites. IUBMB Life 53:85-98.

19. Holehouse, A. S., R. K. Das, J. N. Ahad, M. O. G. Richardson, and R. V. Pappu. 2017. CIDER: Resources to Analyze Sequence-Ensemble Relationships of Intrinsically Disordered Proteins. Biophysical Journal 112:16-21.

20. Pujato, M., C. Bracken, R. Mancusso, M. Cataldi, and M. L. Tasayco. 2005. pH Dependence of Amide Chemical Shifts in Natively Disordered Polypeptides Detects Medium-Range Interactions with Ionizable Residues. Biophysical Journal 89:3293-3302.

21. Mao, A. H., S. L. Crick, A. Vitalis, C. L. Chicoine, and R. V. Pappu. 2010. Net charge per residue modulates conformational ensembles of intrinsically disordered proteins. Proceedings of the National Academy of Sciences of the United States of America 107:8183-8188.

22. Mao, A. H., N. Lyle, and R. V. Pappu. 2013. Describing sequence-ensemble relationships for intrinsically disordered proteins. Biochemical Journal 449:307-318.

23. van der Lee, R., M. Buljan, B. Lang, R. J. Weatheritt, G. W. Daughdrill, A. K. Dunker, M. Fuxreiter, J. Gough, J. Gsponer, D. T. Jones, P. M. Kim, R. W. Kriwacki, C. J. Oldfield, R. V. Pappu, P. Tompa, V. N. Uversky, P. E. Wright, and M. M. Babu. 2014. Classification of Intrinsically Disordered Regions and Proteins. Chemical Reviews 114:6589-6631.

24. Marsh, J. A., B. Dancheck, M. J. Ragusa, M. Allaire, J. D. Forman-Kay, and W. Peti. 2010. Structural Diversity in Free and Bound States of Intrinsically Disordered Protein Phosphatase 1 Regulators. Structure 18:1094-1103.

25. Marsh, J. A., and J. D. Forman-Kay. 2010. Sequence Determinants of Compaction in Intrinsically Disordered Proteins. Biophysical Journal 98:2383-2390.

26. Liu, B., D. Chia, V. Csizmok, P. Farber, J. D. Forman-Kay, and C. C. Gradinaru. 2014. The Effect of Intrachain Electrostatic Repulsion on Conformational Disorder and Dynamics of the Sic1 Protein. Journal of Physical Chemistry B 118:4088-4097.

27. Borgia, A., M. B. Borgia, K. Bugge, V. M. Kissling, P. O. Heidarsson, C. B. Fernandes, A. Sottini, A. Soranno, K. J. Buholzer, D. Nettels, B. B. Kragelund, R. B. Best, and B. Schuler. 2018. Extreme disorder in an ultrahigh-affinity protein complex. Nature 555:61-66.

28. Bugge, K., I. Brakti, C. B. Fernandes, J. E. Dreier, J. E. Lundsgaard, J. G. Olsen, K. Skriver, and B. B. Kragelund. 2020. Interactions by Disorder – A Matter of Context. Frontiers in Molecular Biosciences 7.

29. O'Shea, C., L. Staby, S. K. Bendsen, F. G. Tidemand, A. Redsted, M. Willemoës, B. B. Kragelund, and K. Skriver. 2017. Structures and Short Linear Motif of Disordered Transcription Factor Regions Provide Clues to the Interactome of the Cellular Hub Protein Radical-induced Cell Death1. Journal of Biological Chemistry 292:512-527.

30. Sottini, A., A. Borgia, M. B. Borgia, K. Bugge, D. Nettels, A. Chowdhury, P. O. Heidarsson, F. Zosel, R. B. Best, B. B. Kragelund, and B. Schuler. 2020. Polyelectrolyte interactions enable rapid association and dissociation in high-affinity disordered protein complexes. Nature communications 11:5736.

31. Prestel, A., N. Wichmann, J. M. Martins, R. Marabini, N. Kassem, S. S. Broendum, M. Otterlei, O. Nielsen, M. Willemoës, M. Ploug, W. Boomsma, and B. B. Kragelund. 2019. The PCNA interaction motifs revisited: thinking outside the PIP-box. Cellular and Molecular Life Sciences 76:4923-4943.

32. Millard, P. S., K. Weber, B. B. Kragelund, and M. Burow. 2019. Specificity of MYB interactions relies on motifs in ordered and disordered contexts. Nucleic Acids Research 47:9592-9608.

33. Borg, M., T. Mittag, T. Pawson, M. Tyers, J. D. Forman-Kay, and H. S. Chan. 2007. Polyelectrostatic interactions of disordered ligands suggest a physical basis for ultrasensitivity. Proceedings of the National Academy of Sciences of the United States of America 104:9650-9655.

34. Pak, C. W., M. Kosno, A. S. Holehouse, S. B. Padrick, A. Mittal, R. Ali, A. A. Yunus, D. R. Liu, R. V. Pappu, and M. K. Rosen. 2016. Sequence Determinants of Intracellular Phase Separation by Complex Coacervation of a Disordered Protein. Molecular cell 63:72-85.

35. Kaur, T., M. Raju, I. Alshareedah, R. B. Davis, D. A. Potoyan, and P. R. Banerjee. 2021. Sequence-encoded and composition-dependent protein-RNA interactions control multiphasic condensate morphologies. Nature communications 12:872.

36. Alshareedah, I., M. M. Moosa, M. Raju, D. A. Potoyan, and P. R. Banerjee. 2020. Phase transition of RNA−protein complexes into ordered hollow condensates. Proceedings of the National Academy of Sciences 117:15650.

37. Fisher, R. S., and S. Elbaum-Garfinkle. 2020. Tunable multiphase dynamics of arginine and lysine liquid condensates. Nature communications 11:4628.

38. Yeong, V., J.-w. Wang, J. M. Horn, and A. C. Obermeyer. 2021. Intracellular phase separation of globular proteins facilitated by short cationic peptides. bioRxiv:2021.2007.2008.450573.

39. Chang, L. W., T. K. Lytle, M. Radhakrishna, J. J. Madinya, J. Velez, C. E. Sing, and S. L. Perry. 2017. Sequence and entropy-based control of complex coacervates. Nature communications 8:1273.

40. Knoerdel, A. R., W. C. Blocher McTigue, and C. E. Sing. 2021. Transfer Matrix Model of pH Effects in Polymeric Complex Coacervation. The Journal of Physical Chemistry B 125:8965-8980.

41. Last, M. G. F., S. Deshpande, and C. Dekker. 2020. pH-Controlled Coacervate–Membrane Interactions within Liposomes. ACS Nano 14:4487-4498.

42. Quiroz, F. G., V. F. Fiore, J. Levorse, L. Polak, E. Wong, H. A. Pasolli, and E. Fuchs. 2020. Liquid-liquid phase separation drives skin barrier formation. Science (New York, N.Y.) 367:eaax9554.

43. Lund, M., and B. Jönsson. 2013. Charge regulation in biomolecular solution. Quarterly Reviews of Biophysics 46:265-281.

44. Avni, Y., D. Andelman, and R. Podgornik. 2019. Charge regulation with fixed and mobile charged macromolecules. Current Opinion in Electrochemistry 13:70-77.

45. Burton, R. F. 1988. The protein content of extracellular fluids and its relevance to the study of ionic regulation: Net charge and colloid osmotic pressure. Comparative Biochemistry and Physiology Part A: Physiology 90:11-16.

46. Bah, A., and J. D. Forman-Kay. 2016. Modulation of Intrinsically Disordered Protein Function by Post-translational Modifications. Journal of Biological Chemistry 291:6696-6705.

47. Gil, J., A. Ramírez-Torres, and S. Encarnación-Guevara. 2017. Lysine acetylation and cancer: A proteomics perspective. Journal of Proteomics 150:297-309.

48. Fuhrmann, J., and P. R. Thompson. 2016. Protein Arginine Methylation and Citrullination in Epigenetic Regulation. ACS chemical biology 11:654-668.

49. Bah, A., R. M. Vernon, Z. Siddiqui, M. Krzeminski, R. Muhandiram, C. Zhao, N. Sonenberg, L. E. Kay, and J. D. Forman-Kay. 2015. Folding of an intrinsically disordered protein by phosphorylation as a regulatory switch. Nature 519:106-109.

50. Kennelly, P. J. 2014. Protein Ser/Thr/Tyr Phosphorylation in the Archaea*. Journal of Biological Chemistry 289:9480-9487.

51. Eymann, C., D. Becher, J. Bernhardt, K. Gronau, A. Klutzny, and M. Hecker. 2007. Dynamics of protein phosphorylation on Ser/Thr/Tyr in Bacillus subtilis. PROTEOMICS 7:3509-3526.

52. Bischoff, R., and H. V. J. Kolbe. 1994. Deamidation of asparagine and glutamine residues in proteins and peptides: structural determinants and analytical methodology. Journal of Chromatography B: Biomedical Sciences and Applications 662:261-278.

53. Salehi, A., and R. G. Larson. 2016. A Molecular Thermodynamic Model of Complexation in Mixtures of Oppositely Charged Polyelectrolytes with Explicit Account of Charge Association/Dissociation. Macromolecules 49:9706-9719.

54. Ghasemi, M., and R. G. Larson. 2021. Role of electrostatic interactions in charge regulation of weakly dissociating polyacids. Progress in Polymer Science 112:101322.

55. Fitch, C. A., S. T. Whitten, V. J. Hilser, and E. B. Garcia-Moreno. 2006. Molecular mechanisms of pH-driven conformational transitions of proteins: insights from continuum electrostatics calculations of acid unfolding. Proteins 63:113-126.

56. Hilser, V. J., E. B. Garcia-Moreno, T. G. Oas, G. Kapp, and S. T. Whitten. 2006. A statistical thermodynamic model of the protein ensemble. Chemical Reviews 106:1545-1558.

57. Sharma, U., R. S. Negin, and J. D. Carbeck. 2003. Effects of Cooperativity in Proton Binding on the Net Charge of Proteins in Charge Ladders. The Journal of Physical Chemistry B 107:4653-4666.

58. Simonson, T., J. Carlsson, and D. A. Case. 2004. Proton Binding to Proteins: pKa Calculations with Explicit and Implicit Solvent Models. Journal of the American Chemical Society 126:4167-4180.

59. Shiao, D. D. F., and J. M. Sturtevant. 1976. Heats of binding protons to globular proteins. Biopolymers 15:1201-1211.

60. Anderson, C. F., and M. T. Record. 1993. Salt dependence of oligoion-polyion binding: a thermodynamic description based on preferential interaction coefficients. The Journal of Physical Chemistry 97:7116-7126.

61. Grosberg, A. Y., T. T. Nguyen, and B. I. Shklovskii. 2002. Colloquium: The physics of charge inversion in chemical and biological systems. Reviews of Modern Physics 74:329-345.

62. Roosen-Runge, F., B. S. Heck, F. Zhang, O. Kohlbacher, and F. Schreiber. 2013. Interplay of pH and Binding of Multivalent Metal Ions: Charge Inversion and Reentrant Condensation in Protein Solutions. The Journal of Physical Chemistry B 117:5777-5787.

63. Zhang, F., S. Weggler, M. J. Ziller, L. Ianeselli, B. S. Heck, A. Hildebrandt, O. Kohlbacher, M. W. A. Skoda, R. M. J. Jacobs, and F. Schreiber. 2010. Universality of protein reentrant condensation in solution induced by multivalent metal ions. Proteins: Structure, Function, and Bioinformatics 78:3450-3457.

64. Winkler, R. G., M. Gold, and P. Reineker. 1998. Collapse of Polyelectrolyte Macromolecules by Counterion Condensation and Ion Pair Formation: A Molecular Dynamics Simulation Study. Physical review letters 80:3731-3734.

65. Butler, J. C., T. Angelini, J. X. Tang, and G. C. L. Wong. 2003. Ion Multivalence and Like-Charge Polyelectrolyte Attraction. Physical review letters 91:028301.

66. Angelini, T. E., H. Liang, W. Wriggers, and G. C. L. Wong. 2003. Like-charge attraction between polyelectrolytes induced by counterion charge density waves. Proceedings of the National Academy of Sciences 100:8634.

67. Annunziata, O., L. Paduano, and J. G. Albright. 2007. Multicomponent Diffusion of Lysozyme in Aqueous Calcium Chloride. The Role of Common-Ion Effects and Protein−Salt Preferential Interactions. The Journal of Physical Chemistry B 111:10591-10598.

68. Zheng, Y., and Q. Cui. 2017. Microscopic mechanisms that govern the titration response and pKa values of buried residues in staphylococcal nuclease mutants. Proteins: Structure, Function, and Bioinformatics 85:268-281.

69. Pahari, S., L. Sun, and E. Alexov. 2019. PKAD: a database of experimentally measured pKa values of ionizable groups in proteins. Database 2019.

70. Fossat, M. J., and R. V. Pappu. 2019. q-Canonical Monte Carlo Sampling for Modeling the Linkage between Charge Regulation and Conformational Equilibria of Peptides. The Journal of Physical Chemistry B 123:6952-6967.

71. Mandel, M., and J. C. Leyte. 1972. Some remarks on the titration equation of weak polyacids. Journal of Electroanalytical Chemistry and Interfacial Electrochemistry 37:297-301.

72. Müller, M., L. Wirth, and B. Urban. 2021. Determination of the Carboxyl Dissociation Degree and pKa Value of Mono and Polyacid Solutions by FTIR Titration. Macromolecular Chemistry and Physics 222:2000334.

73. Borukhov, I., D. Andelman, R. Borrega, M. Cloitre, L. Leibler, and H. Orland. 2000. Polyelectrolyte Titration: Theory and Experiment. The Journal of Physical Chemistry B 104:11027-11034.

74. Woodbury, C. P. 1993. The titration curve of weak polyacids. The Journal of Physical Chemistry 97:3623-3630.

75. Fitch, C. A., G. Platzer, M. Okon, B. Garcia-Moreno E., and L. P. McIntosh. 2015. Arginine: Its pKa value revisited. Protein science : a publication of the Protein Society 24:752-761.

76. Bakker, E., and E. Pretsch. 2007. Modern Potentiometry. Angewandte Chemie International Edition 46:5660-5668.

77. Smith, L. A., M. W. Glasscott, K. J. Vannoy, and J. E. Dick. 2020. Enzyme Kinetics via Open Circuit Potentiometry. Analytical Chemistry 92:2266-2273.

78. Gunner, M. R., T. Murakami, A. S. Rustenburg, M. Işık, and J. D. Chodera. 2020. Standard state free energies, not pKas, are ideal for describing small molecule protonation and tautomeric states. Journal of Computer-Aided Molecular Design 34:561-573.

79. Szakács, Z., M. Kraszni, and B. Noszál. 2004. Determination of microscopic acid–base parameters from NMR–pH titrations. Analytical and Bioanalytical Chemistry 378:1428-1448.

80. Bashford, D., and M. Karplus. 1991. Multiple-site titration curves of proteins: an analysis of exact and approximate methods for their calculation. The Journal of Physical Chemistry 95:9556-9561.

81. Onufriev, A., D. A. Case, and G. M. Ullmann. 2001. A Novel View of pH Titration in Biomolecules. Biochemistry 40:3413-3419.

82. Metropolis, N., A. W. Rosenbluth, M. N. Rosenbluth, A. H. Teller, and E. Teller. 1953. Equation of State Calculations by Fast Computing Machines. The Journal of Chemical Physics 21:1087-1092.

83. Platzer, G., M. Okon, and L. P. McIntosh. 2014. pH-dependent random coil 1H, 13C, and 15N chemical shifts of the ionizable amino acids: a guide for protein pKa measurements. Journal of Biomolecular NMR 60:109-129.

84. Gran, G. 1952. Determination of the equivalence point in potentiometric titrations. Part II. Analyst 77:661-671.

85. Gran, G., and A. Johansson. 1981. Automatic titration by stepwise addition of equal volumes of titrant. Part VI. Further extension of the Gran I method for calculation of the equivalence volume in acid-base titrations. Analyst 106:231-242.

86. Yan, J. F. 1965. A Method for the Determination of Equivalence Point in Potentiometric Titrations Using Unequal Volume Increments. Analytical Chemistry 37:1588-1590.

87. Fortuin, J. M. H. 1961. Method for determination of the equivalence point in potentiometric titrations. Analytica Chimica Acta 24:175-191.

88. Nozaki, Y., and C. Tanford. 1967. Examination of titration behavior. In Methods in enzymology. Academic Press. 715-734.

89. Huang, Y., and D. W. Bolen. 1995. Probes of energy transduction in enzyme catalysis. In Methods in enzymology. Academic Press. 19-43.

90. Baker, E. G., G. J. Bartlett, M. P. Crump, R. B. Sessions, N. Linden, C. F. J. Faul, and D. N. Woolfson. 2015. Local and macroscopic electrostatic interactions in single α-helices. Nature Chemical Biology 11:221-228.

91. Peckham, M., and P. J. Knight. 2009. When a predicted coiled coil is really a single α-helix, in myosins and other proteins. Soft Matter 5:2493-2503.

92. Süveges, D., Z. Gáspári, G. Tóth, and L. Nyitray. 2009. Charged single α-helix: A versatile protein structural motif. Proteins: Structure, Function, and Bioinformatics 74:905-916.

93. Wolny, M., M. Batchelor, G. J. Bartlett, E. G. Baker, M. Kurzawa, P. J. Knight, L. Dougan, D. N. Woolfson, E. Paci, and M. Peckham. 2017. Characterization of long and stable de novo single alpha-helix domains provides novel insight into their stability. Scientific Reports 7:44341.

94. Malik, R. U., M. Dysthe, M. Ritt, R. K. Sunahara, and S. Sivaramakrishnan. 2017. ER/K linked GPCR-G protein fusions systematically modulate second messenger response in cells. Scientific Reports 7:7749.

95. Wang, E., and C.-L. A. Wang. 1996. (i,i+ 4) Ion Pairs Stabilize Helical Peptides Derived from Smooth Muscle Caldesmon. Archives of Biochemistry and Biophysics 329:156-162.

96. Fossat, M. J., X. Zeng, and R. V. Pappu. 2021. Uncovering Differences in Hydration Free Energies and Structures for Model Compound Mimics of Charged Side Chains of Amino Acids. The Journal of Physical Chemistry B 125:4148-4161.

97. Nick Pace, C., and J. Martin Scholtz. 1998. A Helix Propensity Scale Based on Experimental Studies of Peptides and Proteins. Biophysical Journal 75:422-427.

98. Myer, Y. P. 1969. The pH-Induced Helix-Coil Transition of Poly-L-lysine and Poly-L-glutamic Acid and the 238-mμ Dichroic Band. Macromolecules 2:624-628.

99. Donten, M. L., and P. Hamm. 2013. pH-jump induced α-helix folding of poly-l-glutamic acid. Chemical Physics 422:124-130.

100. Fonin, A. V., O. V. Stepanenko, A. K. Sitdikova, I. A. Antifeeva, E. I. Kostyleva, A. M. Polyanichko, M. M. Karasev, S. A. Silonov, O. I. Povarova, I. M. Kuznetsova, V. N. Uversky, and K. K. Turoverov. 2019. Folding of poly-amino acids and intrinsically disordered proteins in overcrowded milieu induced by pH change. International Journal of Biological Macromolecules 125:244-255.

101. Mueller-Spaeth, S., A. Soranno, V. Hirschfeld, H. Hofmann, S. Rueegger, L. Reymond, D. Nettels, and B. Schuler. 2010. Charge interactions can dominate the dimensions of intrinsically disordered proteins. Proceedings of the National Academy of Sciences of the United States of America 107:14609-14614.

102. Hofmann, H., A. Soranno, A. Borgia, K. Gast, D. Nettels, and B. Schuler. 2012. Polymer scaling laws of unfolded and intrinsically disordered proteins quantified with single-molecule spectroscopy. Proceedings of the National Academy of Sciences of the United States of America 109:16155-16160.

103. Brucale, M., B. Schuler, and B. Samori. 2014. Single-Molecule Studies of Intrinsically Disordered Proteins. Chemical Reviews 114:3281-3317.

104. Wuttke, R., H. Hofmann, D. Nettels, M. B. Borgia, J. Mittal, R. B. Best, and B. Schuler. 2014. Temperature-dependent solvation modulates the dimensions of disordered proteins. Proceedings of the National Academy of Sciences of the United States of America 111:5213-5218.

105. Ruggeri, F., F. Zosel, N. Mutter, M. Rozycka, M. Wojtas, A. Ozyhar, B. Schuler, and M. Krishnan. 2017. Single-molecule electrometry. Nature Nanotechnology 12:488-495.

106. Holmstrom, E. D., A. Holla, W. Zheng, D. Nettels, R. B. Best, and B. Schuler. 2018. Accurate Transfer Efficiencies, Distance Distributions, and Ensembles of Unfolded and Intrinsically Disordered Proteins From Single-Molecule FRET. Methods in enzymology 611:287-325.

107. Staller, M. V., A. S. Holehouse, D. Swain-Lenz, R. K. Das, R. V. Pappu, and B. A. Cohen. 2018. A High-Throughput Mutational Scan of an Intrinsically Disordered Acidic Transcriptional Activation Domain. Cell systems 6:444-455.e446.

108. Dyla, M., and M. Kjaergaard. 2020. Intrinsically disordered linkers control tethered kinases via effective concentration. Proceedings of the National Academy of Sciences 117:21413.

109. Sørensen, C. S., and M. Kjaergaard. 2019. Effective concentrations enforced by intrinsically disordered linkers are governed by polymer physics. Proceedings of the National Academy of Sciences 116:23124.

110. Greig, J. A., T. A. Nguyen, M. Lee, A. S. Holehouse, A. E. Posey, R. V. Pappu, and G. Jedd. 2020. Arginine-Enriched Mixed-Charge Domains Provide Cohesion for Nuclear Speckle Condensation. Molecular cell 77:1237-1250.e1234.

111. Wiggers, F., S. Wohl, A. Dubovetskyi, G. Rosenblum, W. Zheng, and H. Hofmann. 2021. Diffusion of the disordered E-cadherin tail on β-catenin. bioRxiv:2021.2002.2003.429507.

112. Berg, B. A., and T. Neuhaus. 1992. Multicanonical ensemble: A new approach to simulate first-order phase transitions. Physical review letters 68:9-12.

113. Lewis, M. B. 1957. Relation between the Canonical and Grand Canonical Ensemble. Physical Review 105:348-353.

114. Donnini, S., R. T. Ullmann, G. Groenhof, and H. Grubmuller. 2016. Charge-Neutral Constant pH Molecular Dynamics Simulations Using a Parsimonious Proton Buffer. J Chem Theory Comput 12:1040-1051.

115. Buck, R. P. 1972. Ion selective electrodes, potentiometry, and potentiometric titrations. Analytical Chemistry 44:270-295.

116. Plasson, R., and H. Cottet. 2006. Determination and Modeling of Peptide pKa by Capillary Zone Electrophoresis. Analytical Chemistry 78:5394-5402.

117. Gill, S. J., B. Richey, G. Bishop, and J. Wyman. 1985. Generalized binding phenomena in an allosteric macromolecule. Biophysical Chemistry 21:1-14.

118. Di Cera, E., S. J. Gill, and J. Wyman. 1988. Binding capacity: cooperativity and buffering in biopolymers. Proceedings of the National Academy of Sciences 85:449.

119. Gill, S. J., H. T. Gaud, J. Wyman, and B. G. Barisas. 1978. Analysis of ligand binding curves in terms of species fractions. Biophysical Chemistry 8:53-59.

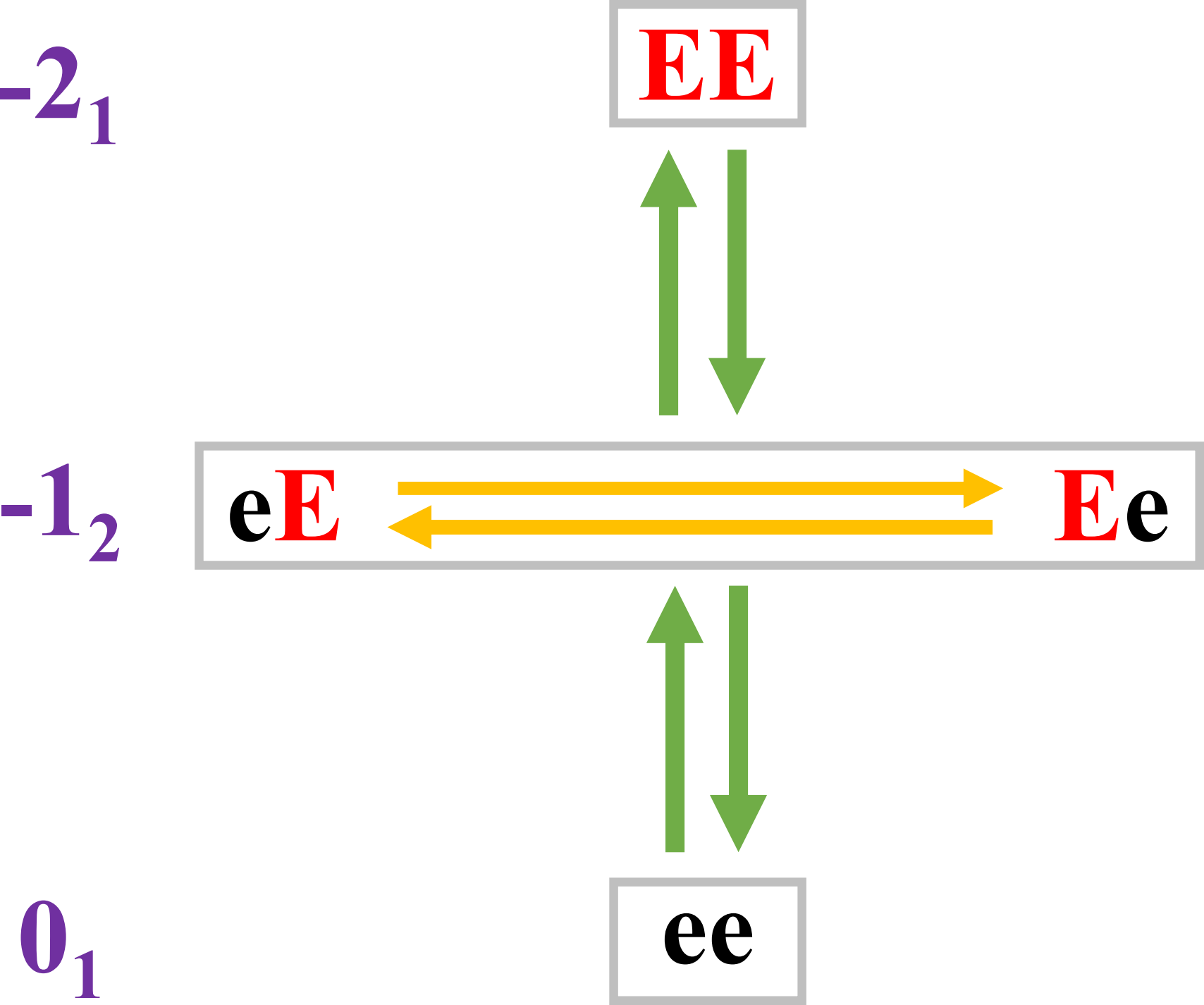
-2₁
EE
-1₂
eE
Ee
0₁
ee

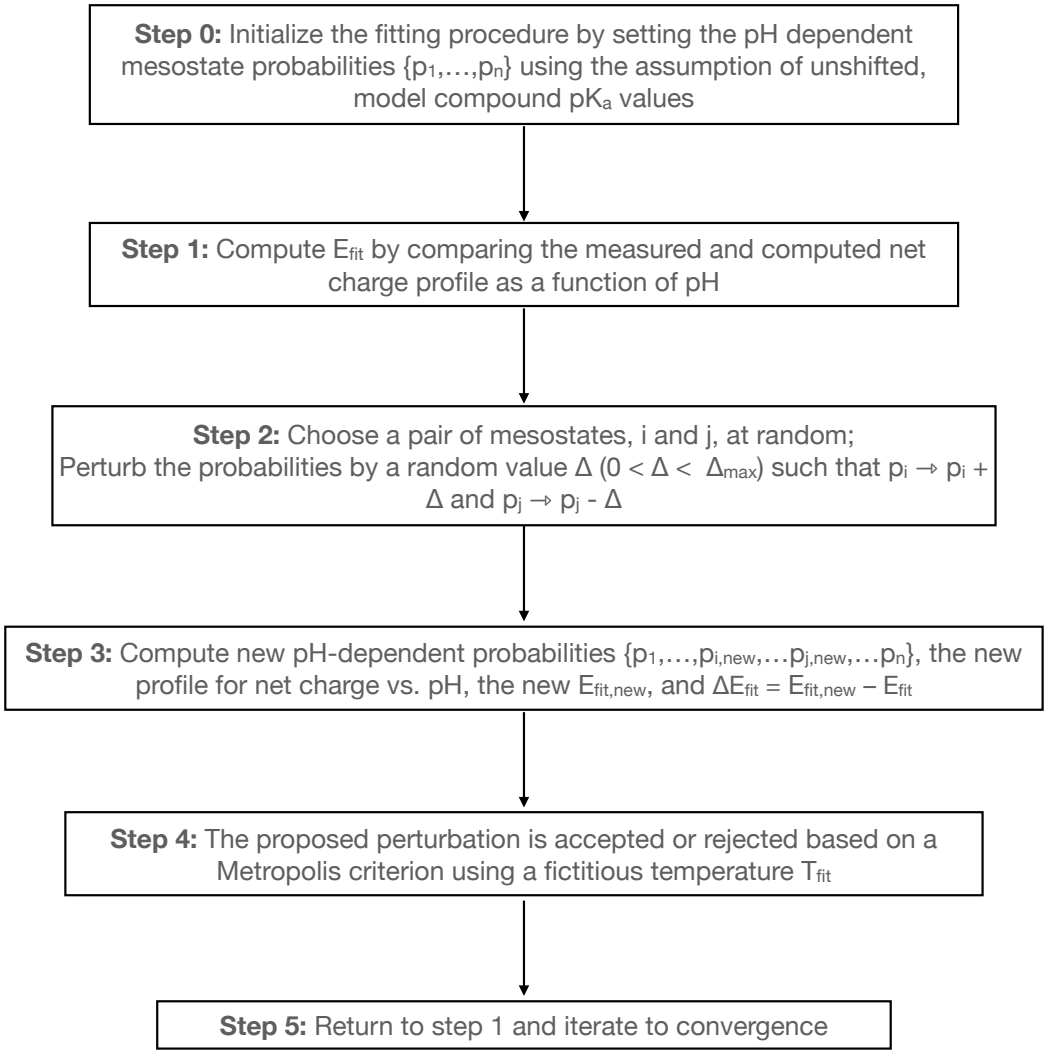
Step 0: Initialize the fitting procedure by setting the pH dependent mesostate probabilities $\{p_1,\ldots,p_n\}$ using the assumption of unshifted, model compound pK_a values
Step 1: Compute E_{fit} by comparing the measured and computed net charge profile as a function of pH
Step 2: Choose a pair of mesostates, i and j, at random; Perturb the probabilities by a random value Δ ($0 < \Delta < \Delta_{max}$) such that $p_i \rightarrow p_i + \Delta$ and $p_j \rightarrow p_j - \Delta$
Step 3: Compute new pH-dependent probabilities $\{p_1,\ldots,p_{i,new},\ldots p_{j,new},\ldots p_n\}$, the new profile for net charge vs. pH, the new $E_{fit,new}$, and $\Delta E_{fit} = E_{fit,new} - E_{fit}$
Step 4: The proposed perturbation is accepted or rejected based on a Metropolis criterion using a fictitious temperature T_{fit}
Step 5: Return to step 1 and iterate to convergence

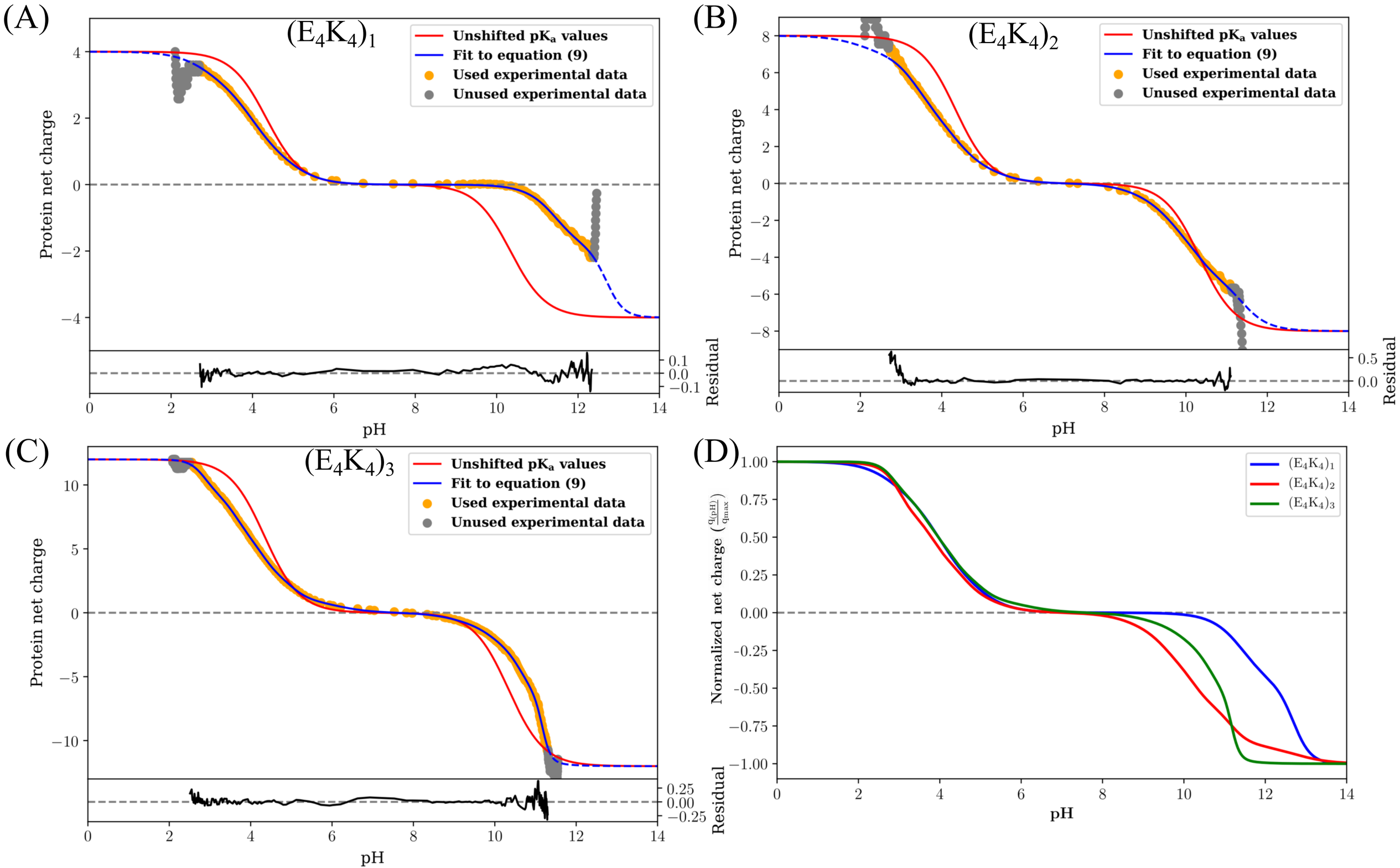
(A)
$(E_4K_4)_1$
Unshifted pK_a values
Fit to equation (9)
Used experimental data
Unused experimental data
Protein net charge
Residual
pH
(B)
$(E_4K_4)_2$
Unshifted pK_a values
Fit to equation (9)
Used experimental data
Unused experimental data
Protein net charge
Residual
pH
(C)
$(E_4K_4)_3$
Unshifted pK_a values
Fit to equation (9)
Used experimental data
Unused experimental data
Protein net charge
Residual
pH
(D)
$(E_4K_4)_1$
$(E_4K_4)_2$
$(E_4K_4)_3$
Normalized net charge $\left(\frac{q(pH)}{q_{max}}\right)$
pH

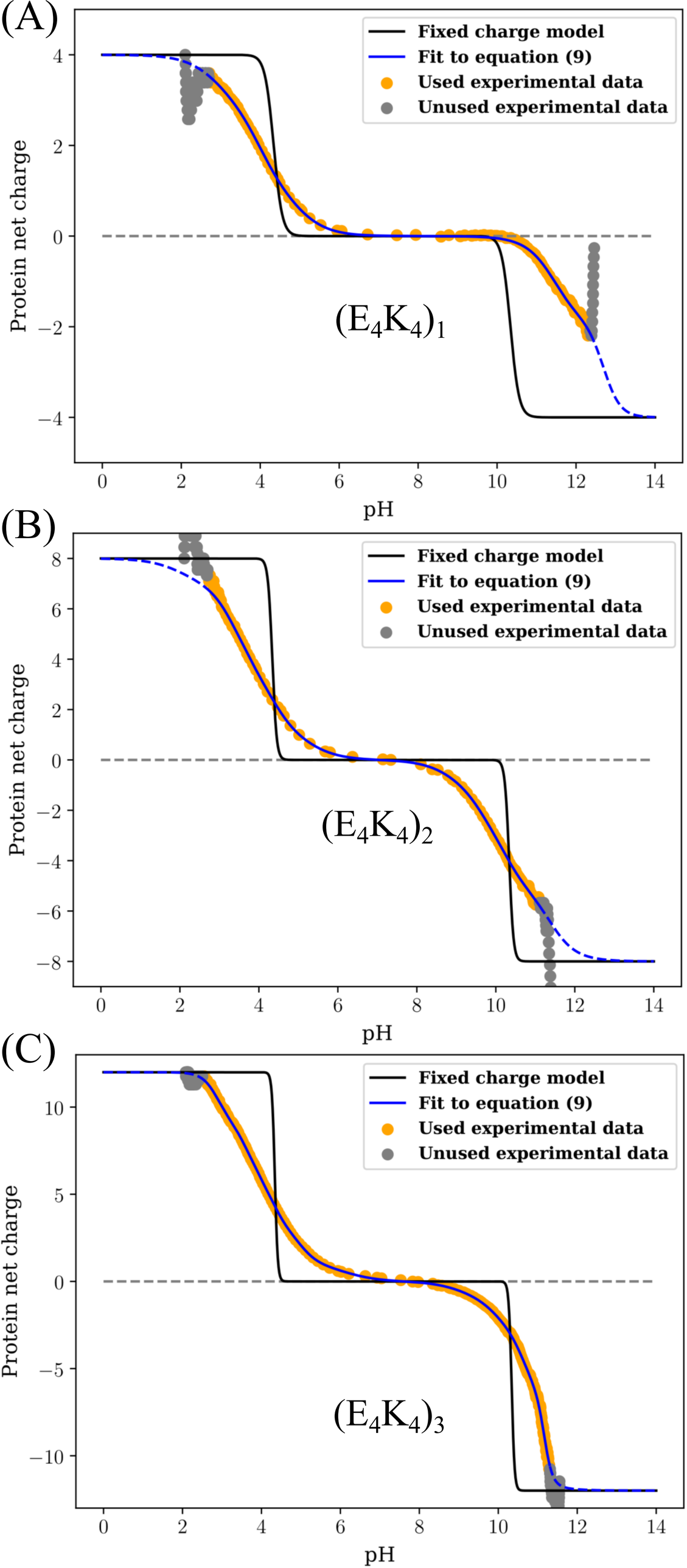
(A)
Fixed charge model
Fit to equation (9)
Used experimental data
Unused experimental data
Protein net charge
pH
$(E_4K_4)_1$
(B)
Fixed charge model
Fit to equation (9)
Used experimental data
Unused experimental data
Protein net charge
pH
$(E_4K_4)_2$
(C)
Fixed charge model
Fit to equation (9)
Used experimental data
Unused experimental data
Protein net charge
pH
$(E_4K_4)_3$

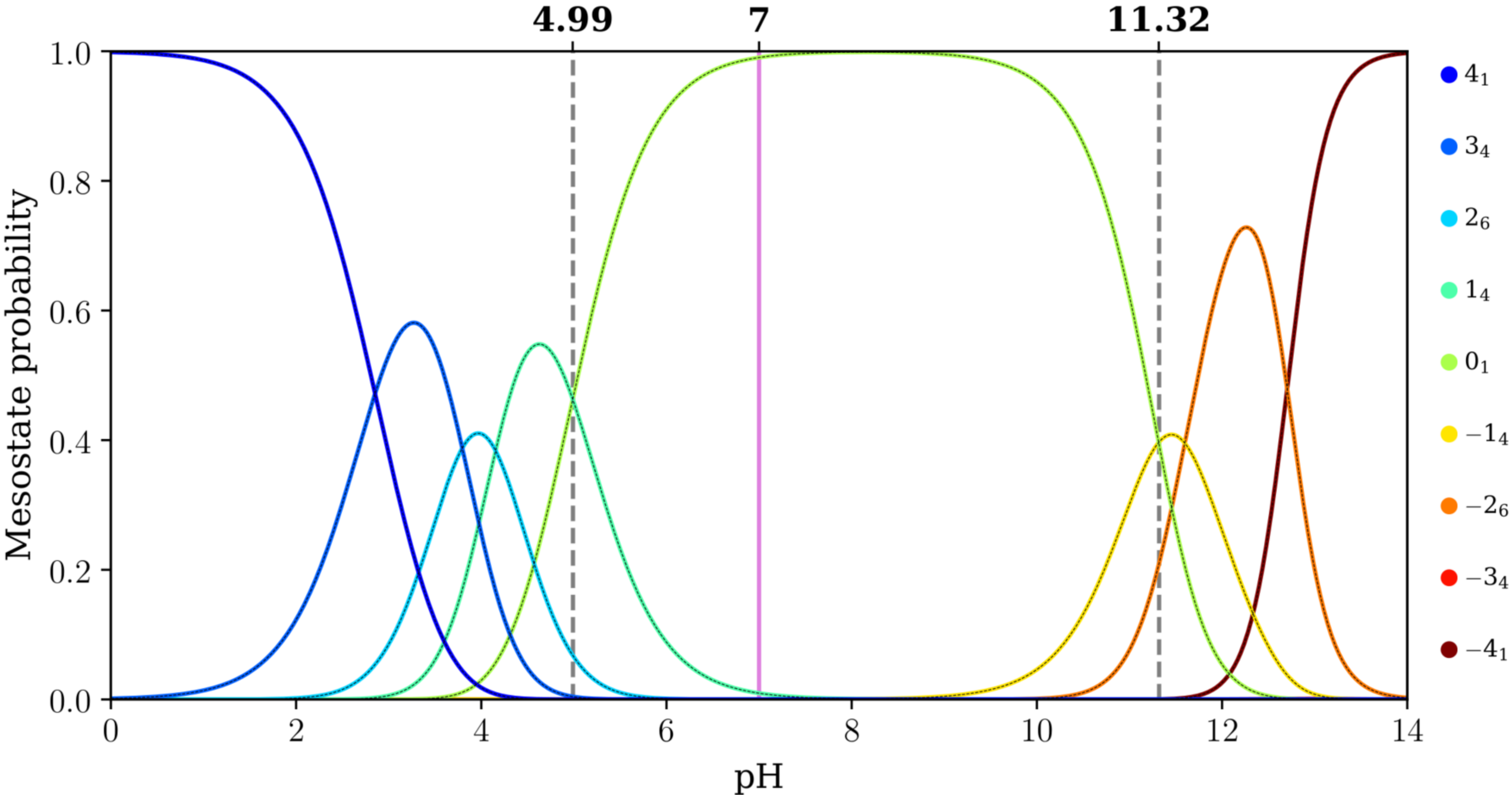
4.99
7
11.32
1.0
0.8
0.6
0.4
0.2
0.0
Mesostate probability
0
2
4
6
8
10
12
14
pH
4_1
3_4
2_6
1_4
0_1
-1_4
-2_6
-3_4
-4_1

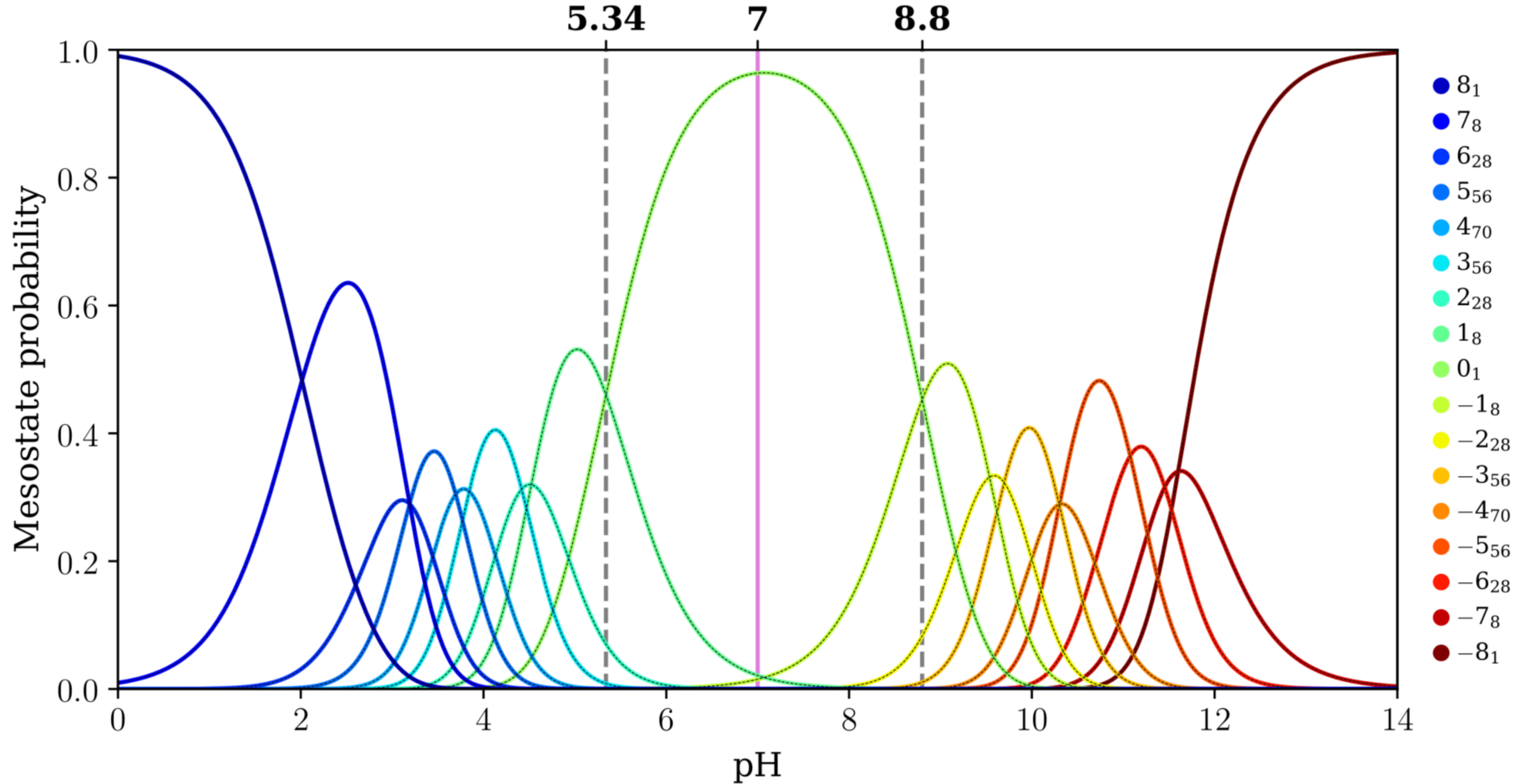
5.34
7
8.8
1.0
0.8
0.6
0.4
0.2
0.0
Mesostate probability
0
2
4
6
8
10
12
14
pH
8_1
7_8
6_{28}
5_{56}
4_{70}
3_{56}
2_{28}
1_8
0_1
-1_8
-2_{28}
-3_{56}
-4_{70}
-5_{56}
-6_{28}
-7_8
-8_1

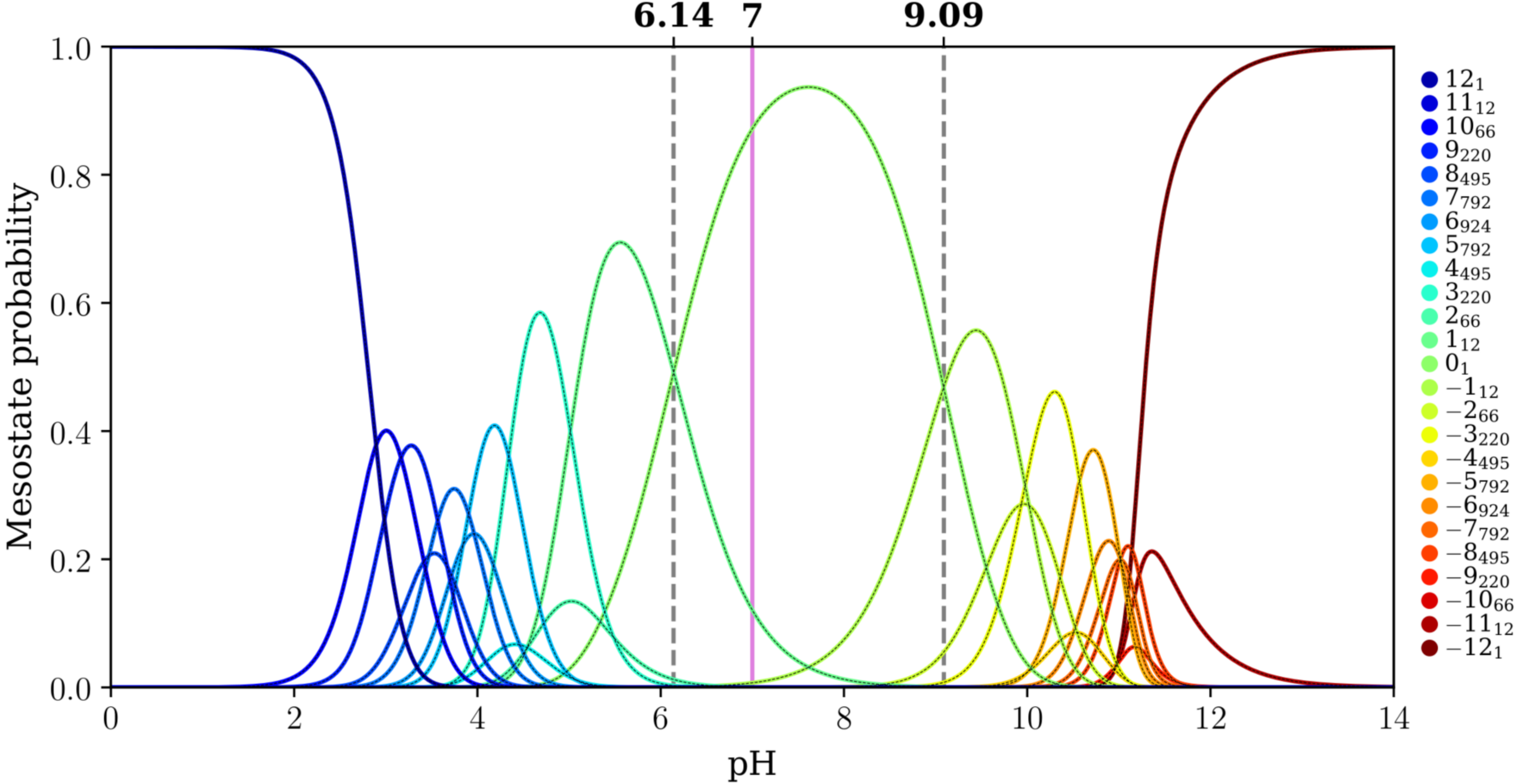
6.14
7
9.09
Mesostate probability
pH
0.0
0.2
0.4
0.6
0.8
1.0
0
2
4
6
8
10
12
14
12_1
11_{12}
10_{66}
9_{220}
8_{495}
7_{792}
6_{924}
5_{792}
4_{495}
3_{220}
2_{66}
1_{12}
0_1
-1_{12}
-2_{66}
-3_{220}
-4_{495}
-5_{792}
-6_{924}
-7_{792}
-8_{495}
-9_{220}
-10_{66}
-11_{12}
-12_1

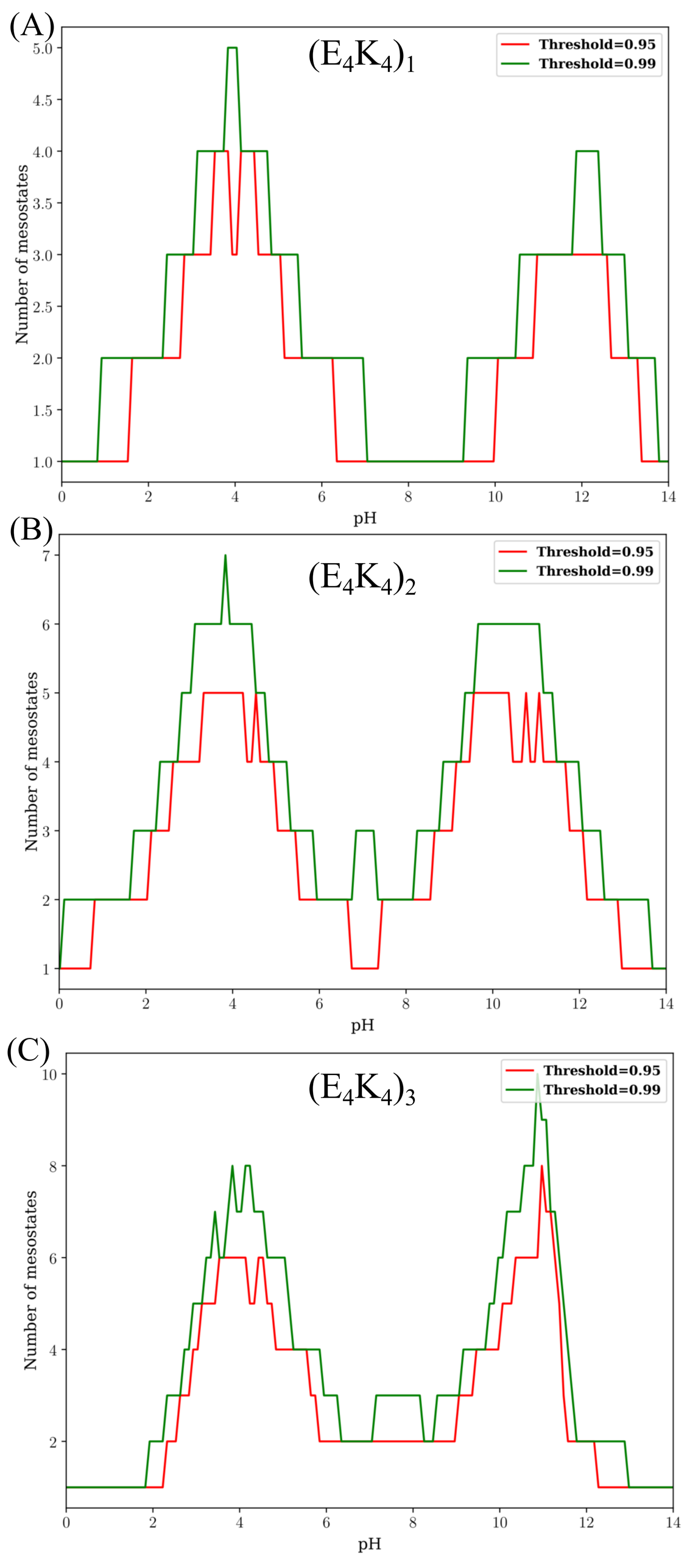
(A)
$(E_4K_4)_1$
Threshold=0.95
Threshold=0.99
Number of mesostates
pH
(B)
$(E_4K_4)_2$
Threshold=0.95
Threshold=0.99
Number of mesostates
pH
(C)
$(E_4K_4)_3$
Threshold=0.95
Threshold=0.99
Number of mesostates
pH